AD-A053 291 RICE UNIV HOUSTON TEX F/G 8/14
STUDY OF PLASMA FLOW NEAR THE EARTH'S PLASMAPAUSE.(U)
NOV 77 M HAREL, R A WOLF, P H REIFF F19628-77-C-0012
UNCLASSIFIED AFGL-TR-77-0286 NL

1 OF 1
AD A053291

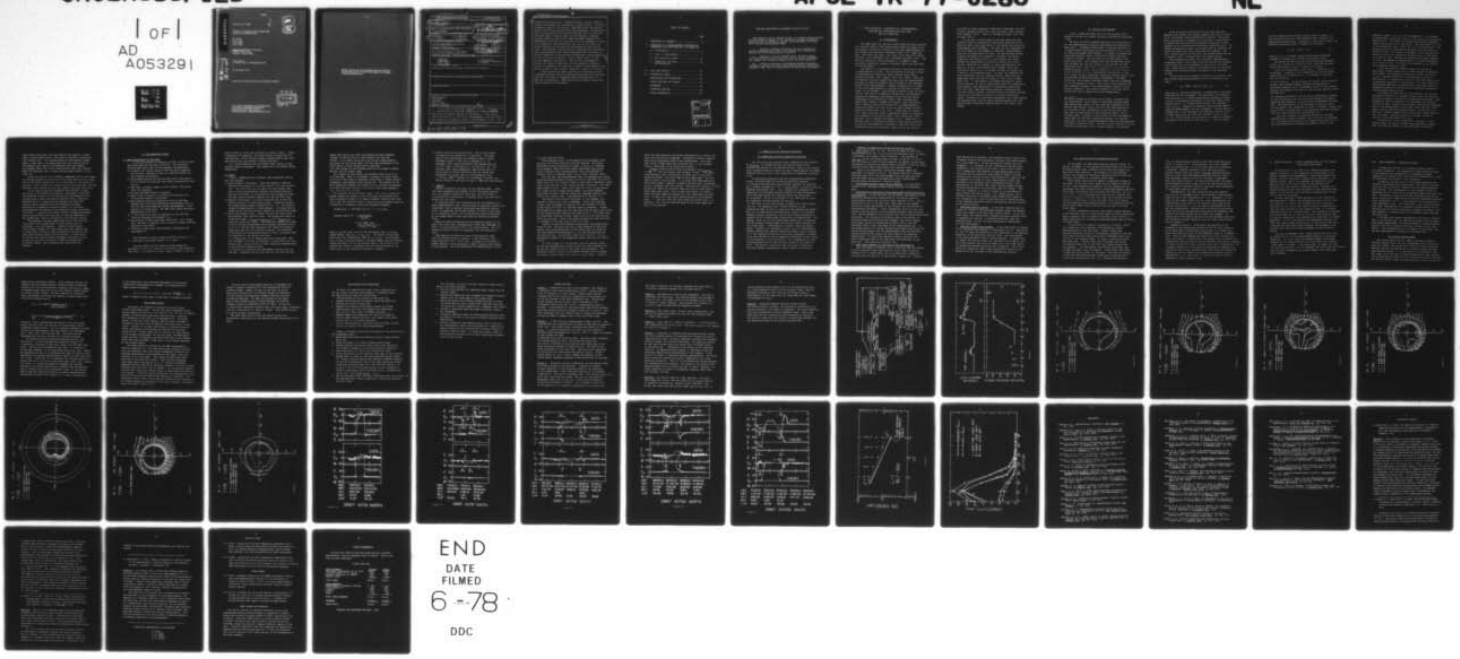

END
DATE FILMED
6-78
DDC

AFGL-TR-77-0286

STUDY OF PLASMA FLOW NEAR THE EARTH'S PLASMAPAUSE

M. Harel
R.A. Wolf
P.H. Reiff
H.K. Hills

William Marsh Rice University
6100 S. Main Street
Houston, Texas 77005

Final Report
1 October 1976 - 30 September 1977

28 November 1977

Approved for public release; distribution unlimited

AIR FORCE GEOPHYSICS LABORATORY
AIR FORCE SYSTEMS COMMAND
UNITED STATES AIR FORCE
HANSCOM AFB, MASSACHUSETTS 01731

Unclassified

SECURITY CLASSIFICATION OF THIS PAGE (When Data Entered)

(19) **REPORT DOCUMENTATION PAGE**

READ INSTRUCTIONS BEFORE COMPLETING FORM

(18) 1. REPORT NUMBER: AFGL-TR-77-0286

2. GOVT ACCESSION NO

3. RECIPIENT'S CATALOG NUMBER

(6) 4. TITLE (and Subtitle): STUDY OF PLASMA FLOW NEAR THE EARTH'S PLASMAPAUSE.

(9) 5. TYPE OF REPORT & PERIOD COVERED: Final report. 1 Oct 76-30 Sep 77

6. PERFORMING ORG. REPORT NUMBER

(10) 7. AUTHOR(s): M. Harel, P. H. Reiff, R. A. Wolf, H. K. Hills

(15) 8. CONTRACT OR GRANT NUMBER(s): F19628-77-C-0012, F19628-77-C-0005

9. PERFORMING ORGANIZATION NAME AND ADDRESS: ~~William Marsh~~ Rice University, 6100 S. Main St. Houston, Texas 77005

(16) 10. PROGRAM ELEMENT, PROJECT, TASK AREA & WORK UNIT NUMBERS: 61102F, 2311G201 (17) G2

(11) 11. CONTROLLING OFFICE NAME AND ADDRESS: Air Force Geophysics Laboratory, Hanscom AFB, Massachusetts 01731, Contract Monitor: Michael Smiddy (PHR)

12. REPORT DATE: 28 November 1977

13. NUMBER OF PAGES: 56

14. MONITORING AGENCY NAME & ADDRESS (if different from Controlling Office): (12) 58 p.

15. SECURITY CLASS. (of this report): Unclassified

15a. DECLASSIFICATION DOWNGRADING SCHEDULE

16. DISTRIBUTION STATEMENT (of this Report)

Approved for public release; distribution unlimited.

17. DISTRIBUTION STATEMENT (of the abstract entered in Block 20, if different from Report)

18. SUPPLEMENTARY NOTES

19. KEY WORDS (Continue on reverse side if necessary and identify by block number)

Magnetosphere
Ionosphere
Substorm
Ring Current
Electric Fields

20. ABSTRACT (Continue on reverse side if necessary and identify by block number)

We have now successfully completed our first simulation run of a magnetospheric substorm. Our computer program has been developed to simulate aspects of the behavior of the closed-field-line portion of the earth's magnetosphere, and the auroral and subauroral ionosphere, during a magnetospheric event. The

DD FORM 1 JAN 73 1473 EDITION OF 1 NOV 65 IS OBSOLETE

Unclassified

SECURITY CLASSIFICATION OF THIS PAGE (When Data Entered)

* was successfully completed. 305 750

cont. program self-consistently, computes electric fields, electric currents and plasma flow velocities in these regions. The basic program has been run for several idealized cases, and various output and plotting routines have been developed. Electron-flux data and polar-cap electric-field data from the S3-2 satellite have been used to specify input for the program. Computed electric fields in the auroral zone have been compared with measurements from the S3-2 satellite, and the agreement is found to be reasonably good considering that this is our first try. Various features of the data are interpreted in terms of the model. The computed time-evolution of the particle distribution near geosynchronous orbit agrees reasonably well with what is normally observed by McIlwain and collaborators during substorms. At the end of the simulation (3 hours after onset), a ring current appears to be forming. This initial confrontation between the computer model and the data suggests a number of changes in boundary conditions and a number of improvements that should be made in the program. These are listed in the report.

A simple method has been developed for estimating height-integrated Pedersen and Hall conductivities using S3-2 electron-flux data and certain ionospheric-model calculations of M. H. Rees and collaborators. DMSP photos have provided limited but useful conductivity information.

TABLE OF CONTENTS

ORIGINAL OBJECTIVES OF CONTRACT F19628-77-C-0012

The objective of the contract study is to develop quantitatively accurate computer models of the interaction between the magnetosphere and the ionosphere at auroral zone and middle latitudes. This includes the following tasks:

I. Develop a computer simulation for one or more well-observed magnetospheric events, and compare with observations made by Air Force satellites S3-2 and S3-3.

II. Develop an initial computer model including plasma flow along magnetic field lines into and out of the ionosphere, and compare with observations made by an Air Force satellite.

III. Develop techniques for estimating height-integrated ionospheric conductivity using DMSP photographs and simultaneous Chatanika radar and S3-2 observations of the auroral ionosphere.

I. FIRST OBJECTIVE: SIMULATION OF A MAGNETOSPHERIC SUBSTORM AND COMPARISON WITH DATA FROM THE S3-2 SATELLITE

A. Introduction

For some years now, the Rice theory group has been involved in a project aimed at self-consistently computing plasma flows and electric fields and currents in the inner magnetosphere and the auroral and subauroral ionosphere [Wolf, 1970; Jaggi and Wolf, 1973; Wolf and Jaggi, 1973; Wolf, 1974; Wolf, 1975; Harel and Wolf, 1976; Southwood, 1977; Southwood and Wolf, 1977]. The work has centered on the development of a computer model, although a substantial amount of analytic theory has also come out of the effort.

Our approach to the problem follows a long chain of papers in magnetospheric physics. The formulation of the basic ideas of magnetospheric convection dates from the early 1960's [Axford and Hines, 1961; Dungey, 1961; Cole, 1961]. Some sort of effective friction between the solar wind and magnetosphere was seen to cause antisunward flow of plasma in the outermost region of the magnetosphere; a general sunward flow of plasma in the inner magnetosphere is required to maintain a steady state, on the average. (See reviews by Axford (1969) and Stern (1977)). The role of ionospheric conductivity and Birkeland currents in regulating this sunward return flow was partly understood in the mid-sixties [Fejer, 1964; Karlson, 1963; Block, 1966]. Schield, Freeman and Dessler (1969) developed a fairly complete qualitative picture of the magnetospheric-convection system, and the picture was made clearer and more precise by Vasyliunas (1970, 1972). Aside from our group's work, there have been several theoretical efforts at quantitative modeling of the system [Swift, 1971; Vasyliunas, 1972; Mal'tsev, 1974; Yasuhara and Akasofu, 1977]. There also is another class of mathematical models of the electric field in the auroral and subauroral ionosphere; these very useful and convenient models are relatively simple and do not involve

solutions to large systems of differential equations; they are, instead, derived directly from data [McIlwain, 1974; Volland, 1975; Heppner, 1977]. (See also reviews by Stern (1977) and Kivelson (1977).)

In our view, the Rice work is the most persistent and complete effort at quantitative theoretical modeling of the electric fields and plasma flows in the auroral and subauroral magnetosphere and ionosphere. Our work has now progressed to the point where we can attempt to simulate a magnetospheric event and do comparisons with data. By now the most obvious physical processes are included in our model, and direct comparison with detailed data is now possible and useful. Because the magnetospheric-convection system has no well-defined steady-state, average, or quiet configuration, the best way to get a good confrontation between theory and observation seems to be to attempt to model the system for a specific, well-observed event. We have just completed our first simulation run for a specific event, namely the substorm-type event that had its onset at 1000 UT on 19 September 1976. In this report, we briefly describe the logic of our program, the way in which we did this first simulation, some results, some comparisons of theoretical predictions with S3-2 data, some preliminary physical interpretations, and some lessons learned. We also discuss two closely related topics that are directly related to contract objectives, namely, a program for following plasmasphere flux tubes through the observed event and our nearly developed method for estimating height-integrated conductivities in the auoral ionosphere.

B. Logic of the Program

Figure 1 shows the basic logic of our program, which generally follows the logical structure outlined by Vasyliunas (1970).

We start at the box labeled "Hot-Particle Distribution". Let the magnetospheric particle distribution be prescribed at some time t. A magnetic-field model is derived such that it is approximately consistent with force balance ($\underset{\sim}{j} \times \underset{\sim}{B} - \underset{\sim}{\nabla} p \simeq 0$) for the given plasma distribution*. In order to estimate the storm-time magnetic field, a fictitious current loop was turned on at onset. The resulting ΔB is then added to the quiet-time field. This current loop lies outside the region that we model and its only purpose is to estimate the substorm-time field. This loop, a modification of one used by McPherron et al. (1973), has an equatorial eastward current across the tail at 50 R_E (representing interruption of the tail current during a substorm), Birkeland currents down to the northern-and southern-hemisphere ionospheres, a westward electrojet, and another Birkeland current from the ionosphere out to the equatorial plane. This type of loop simulates the most important changes in the magnetospheric magnetic field during a substorm. The current strength in the loop can be varied with time to agree with ground magnetograms.

---

*We have a scheme for deriving such a model, starting from the Olson-Pfitzer (1974) model or some other standard model. Some preliminary results of this type were presented at the Seattle IAGA meeting, and we now have some understanding of the relatively minor differences in the results that come from using an approximately self-consistent model, over a standard model. However, we were unable to use this magnetic-field model for the event simulation because, for substorm conditions, the self-consistent-magnetic-field routine generated substantial numerical noise. For the current simulation run, we used the Olson-Pfitzer (1974) analytic magnetic field model.

Given an initial distribution of hot particles and a magnetic-field model, the program computes the initial distribution of gradient- and curvature-drift currents. The pitch-angle distribution is assumed to be isotropic. Specifically, we assume that the time for pitch-angle scattering is short compared to the time scale for convecting around the earth. We neglect polarization drift, which means that our treatment is valid only when total drift velocities are subsonic. The total current density is the sum of the current densities due to gradient drift, curvature drift and magnetization.

The divergence of these drift currents, appropriately integrated along a field line, gives the density of Birkeland current down into the ionosphere at the foot of the field line. Magnetization current is divergence-free, so that only gradient and curvature drifts contribute to the Birkeland current.

We now enter the ionospheric portion of the logical loop. The current-conservation equation $\nabla \cdot \underset{\sim}{j} = 0$ is written in the form

$$\nabla_h \cdot \int dh [\underset{\sim}{g} \cdot (-\nabla V + \underset{\sim}{v}_n \times \underset{\sim}{B})] = j_{\parallel} \quad , \qquad (1)$$

where the $\nabla_h \cdot$ operator represents a 2-dimensional, horizontal divergence in the ionosphere, $\int dh$ represents an integration over altitude h, $\underset{\sim}{g}$ = tensor representing ionospheric conductivity, V = electrostatic potential in the rest frame of the rotating earth, $\underset{\sim}{v}_n$ = neutral-wind velocity, $\underset{\sim}{B}$ = magnetic field and $j_{\parallel}$ = density of Birkeland current being dumped from the magnetosphere into the ionosphere. We have implicity assumed that in the ionosphere the potential electric field is much larger than the induction electric field, so that $\underset{\sim}{E} \approx -\nabla V$. We are working on inclusion of a realistic neutral-wind model, but for now we just set $\underset{\sim}{v}_n = 0$. We also assume

that the communication between E and F layers is good, i.e., the portion of the field lines between E and F layers is an approximate equipotential. Equation (1) can then be shown (e.g. Rishbeth and Garriott 1969) to simplify to the form

$$\nabla_h \cdot [\underset{\sim}{\Sigma} \cdot (-\nabla_h V)] = j_{\parallel} , \qquad (2)$$

where $\underset{\sim}{\Sigma}$ is a 2 x 2 tensor representing height-integrated ionospheric conductivity, including dip-angle effect.

Our method for deriving the height-integrated conductivities, as a function of latitude, local time and universal time is described in detail in section III below.

Given the conductivity tensor and $j_{\parallel}$, equation (2) is an elliptic equation in two dimensions that can be solved numerically for the potential V. Our boundary conditions are the following:

(i) zero electric current across the equator (this condition follows from assumed symmetry between the hemispheres, a reasonable assumption for 19 September, which is near equinox; actually the condition we apply is that of zero current across latitude 21°);

(ii) specified potential V on the polar cap boundary (because of the irregularities of the polar cap boundary we actually specified the potential on a circle that encompasses the polar cap). The distribution of the potential around this curve has the general form suggested by Figure 1 of Heelis, Hanson, and Burch (1976); the magnitude of the potential drop was estimated from real-time observations (see section I-C).

Once the ionospheric potential distribution has been determined for a given universal time by solution of equation (2), the potential distribution is mapped along field lines to give the distribution of potential electric fields in the

equatorial plane. For this run we assumed $E_{||} = 0$ (although we expect that a potential drop of a few kV will not change the results much). We intend to include field-aligned potential drops in our simulations in the future. The total electric field in the equatorial plane is the sum of two contributions: the potential electric field mentioned above, and the induction electric field. The latter is included in our calculation by means of letting the equatorial crossing point of the field line vary in time. Because the magnetic-field model changes in time, the equatorial mapping point of a given ionospheric point moves in time. This motion corresponds to $\underline{E} \times \underline{B}$ drift in an induction electric field.

Given the potential electric field, the motion of equatorial crossing points due to induction, and the magnetic-field model, the program calculates total drift velocities ($\underline{E} \times \underline{B}$ + gradient+curvature) for plasma-sheet particles. Specifically, it computes the motion of the inner edge of the plasma-sheet electron-ion distribution. For this simulation, the program kept track of the motions of the inner edge of 5 different energies of electrons and 10 different energies of singly-charged positive ions.

The number of particles per unit magnetic flux and the entropy per particle are assumed uniform across the region of our outer boundary that supplies plasma-sheet particles. This assumption, made for simplicity in the absence of strongly conflicting data, implies that Birkeland currents are generated only at the plasma sheet's inner edge [Jaggi and Wolf, 1973], aside from the effects of precipitation. As they drift, a particle's thermal energy varies as flux tube volume $\int ds/B$ to the -2/3 power. Particle density, of course, varies as $(\int ds/B)^{-1}$, provided there is no loss.

Precipitative loss of electrons is included in the present model by making a conventional assumption, namely that the electrons suffer strong pitch-angle scattering.

Under these conditions, the inner edge of the electron plasma sheet is often essentially a precipitation boundary [Vasyliunas, 1968; Kennel, 1969]. We include erosion of the electron plasma sheet's inner edge in an approximate way that involves having the computer keep track of two boundaries for each energy: one boundary where 25% of the electrons have been lost, another where 75% have been lost. Proton loss has been ignored in this first run.

Given the velocities of different components of the inner edge, the program advances the position of the inner edge for each component by the amount appropriate to one time step δt (30 seconds in practice); this finishes the logical loop for one time step. The program then starts around the loop for another time step, and so on.

In the actual numerical procedure, the program, in every time step, reinterpolates the magnetic field model, recalculates Birkeland currents for the new particle and magnetic-field configuration, reads the observed electron fluxes, readjusts Pedersen and Hall conductivities, readjusts the polar cap potential drop, re-solves the two-dimensional elliptic equation for ionospheric potentials using a 21 x 28 grid, reinterpolates the mapping to the equatorial plane, calculates corotation, curvature and gradient drifts, recomputes boundary velocities and moves the inner edge of various components of the plasma-sheet (what we represent by 400 boundary points).

The problem is further complicated by the fact that the inner edge of the plasma sheet is often rather thin (of the order of one grid spacing). Electric fields vary by large factors through this edge region and often change sign. In other words, electric fields generated by one part of the inner edge strongly affect particle motions in other parts. To include this sub-grid-scale phenomenon accurately in the program, we have had to include a rather intricate self-correction scheme, which substantially complicates the program.

C. The simulation itself

1. Basic description of the event

In the long process of choosing an event, we had to scan many data bases for the years 1975-1976. The following criteria were used (some of them somewhat contradictory):

a) a typical and clearly defined (with one major expansion and recovery) substorm so that our simulation model will be as general as possible.
b) Long enough duration so that we could have a few passes of S3-2 during the substorm (this partly contradicts criterion a).
c) Good data in several passes of S3-2 (before, during and after the substorm).
d) As many good DMSP photos as possible.
e) Being close to equinox (to minimize difficulties with our untilted magnetic field model).
f) North America being at nighttime so that we can make maximum use of the AFGL midlatitude magnetometer chain as well as other North-American ground magnetometers. This implies a UT restriction. The AFGL chain began operations approximately July 1976.
g) A date that is as early as possible so that the data could be processed and shipped to us.
h) Availability of data from other satellites: S3-3, TRIAD, ISIS, and AE-C if possible (will be used in future detailed analysis of the event)
i) Position of ATS-6 near local midnight (conflicts with requirement f).

The substorm we finally chose satisfied criteria b, c, e, f, g and partly satisfied criteria a, d, and h.

Figure 2A shows the Fort Churchill magnetogram for September 19, 1976 as a function on Universal Time (Greenwich Mean Time). The substorm we have chosen to model is the one

with an onset at 10:00 and a duration of about 5 hours. A small disturbance was observed a few hours earlier (around 0600 UT), unfortunately, two of the S3-2 passes occurred during that time span and we thus have chosen to ignore that data.

It is quite possible that our chosen event, being so long, involves several substorms. This however will not change things drastically.

2. Input

Figure 1 summarizes the different input parameters that go into our program.

a) Ground magnetic variations. These are needed in order to estimate the strength of our polar current loop (see section I-B). For this first run, we chose our loop current such that it would approximately reproduce the ground variation observed at Boulder, as a function of time through the event. The peak current strength deduced this way was 2×10^6 amps.

b) Magnetic field model. For this simulation run we used the analytic version of Olson-Pfitzer model. Though not perfect, this approximation appears adequate for $L < 10$. For larger L values the approximation is less adequate. In future work we intend to use the more accurate version of Olson-Pfitzer model.

c) Polar cap potential drop. Figure 2B gives the cross polar-cap potential drop from S3-2 data. The values were obtain by integrating $\int \underline{E} d\underline{s} = \int E_{forward} \, v_{satellite} \, dt \approx \Sigma E_{forward} \, \Delta L$ along the satellite's orbit. The polar-cap boundary was taken to be at the most equatorward field reversal observed (mostly at $70 \pm 3^\circ$) and the boxes represent the ranges of potentials found when more than one reversal occurred. The following difficulties were encountered trying to reach a potential drop as a function of time during the event:

(i) Although most of the passes were mainly dawn-dusk, some only "skimmed" the polar cap boundary (in particular the first and the last) giving rise to an error (generally underestimate) in the resulting potential drop.

(ii) We have no potential-drop measurement between 0640 and 0940 GMT. Combined with the fact that the 0450 and 0620 GMT

passes were during the small disturbance and were therefore ignored, we had virtually no data between 0450 and 1000 (onset). As a result we believe that we have underestimated the length of the growth phase for this run, represented by the solid curve in Figure 2B from 0900 to 1000 GMT.
(iii) The values for the recovery phase do not suggest a smooth decline, but are rather jumpy.

As a result we have chosen the potential drop to be 20 kV till 0900 GMT. Then, we increased it linearly to reach a peak of 80 kV at 1040 (peak of substorm) after which it stays constant throughout the recovery phase (Figure 2B). The results of the first simulation suggest our results can be improved considerably by a more judicious choice for the fit to this input parameter (see chapter on future work).

d) S3-2 electron fluxes and DMSP photos. All the S3-2 satellite passes (Figure 2B) except for the 1040 pass also provided good data on electron fluxes in 16 energy channels, covering the range .08-17 keV. We converted these to energy flux and average energy as a function of latitude by using the following formulas:

$$\text{Energy flux} \equiv \int \tfrac{1}{2}mv^3\cos\theta\, f(\underline{v})\, d^3v \overset{\sim}{\sim} \pi \sum_i \eta C_i (\Delta E)_i$$

$$\text{Average Energy } \langle E\rangle \equiv \frac{\int \tfrac{1}{2}mv^2 f(v) d^3v}{\int f(\underline{v}) d^3v} \overset{\sim}{\sim} \frac{\Sigma (C_i/\sqrt{E_i})\ (\Delta E)_i}{\Sigma (C_i/E_i)^{3/2})\,(\Delta E)_i}$$

where C_i is the count rate for the $i^{\underline{th}}$ energy step, E_i is the center energy, and $(\Delta E)_i$ is $(E_{i+1}-E_i)$. The factor η transforms count rate into differential flux, by $j_i = \eta C_i/E_i$. We proceeded then to take a running average of electron energy flux and average energy for every 0.5° in the auroral region. We finally interpolated the values in universal time and converted them to conductivities by the procedure described in chapter 3.

e) Initial hot-particle distribution. The initial plasma configuration we started with is arbitrary. The inner edge of the plasma-sheet was assumed to have a finite thickness (about 0.7 Re) and is located at L $\sim$ 10. Isotropic pitch angle distribution was assumed with n_e = 1.5 cm^{-3}, kT_e = 1.5 keV and kT_i = 4.5 keV at L$\sim$ 10. Unlike the other input parameters, these values were inserted once as initial conditions and the values were calculated at a later time with the assumption that $\lambda_k = \varepsilon_k/q_k \times (\int \frac{ds}{B})^{2/3}$ serves as an adiabatic invariant. (ε_k = kinetic energy of particles of type κ, $\int \frac{ds}{B}$ = flux tube volume).

3. Results

Section 2 describes the logic of our computer model. Given the input parameters and assumed initial hot-plasma distribution, our program follows the long logic chain of figure 1 to find particle distribution 30 seconds later, and then starts around the loop again.

To stimulate quiet time conditions we ran our program for 2 hours magnetospheric time, starting from an arbitrary initial configuration, with an applied cross-polar-cap potential drop of 20 kV. As expected, the plasma drifted in closer to the earth, as it configured itself so as to shield the region equatorward of the plasma sheet's inner edge from the convection electric field.

Figure 3a shows the mapping of the potential pattern at the end of the quiet time (corresponding to 0900 GMT, September 19, 1976), to the equatorial plane of the magnetosphere. Only the convection electric field is displayed, not the corotation field.

Inner edges are plotted for three of the particle types that the program follows in detail: $\sim$2 keV electrons, zero energy particles and $\sim$ 30 keV ions. Although the shielding is almost complete on the nightside, a small electric field exists on the dayside. Note that boundaries are approximately circles

8 R_E away from the earth.

The outermost circle is the mapping of our boundary curve over which the 20 keV potential drop was applied. The plasma and electric-field configuration shown in Figure 3a, although quite relaxed, would have more nearly approached equilibrium, given a few more hours magnetospheric time (and hundreds of dollar's worth of computer time!) [e.g., Harel and Wolf, 1976].

For the next hour magnetosphere time, we increased the cross-polar-cap potential drop to reach ∿60 keV at 1000 GMT, the time of onset (Fig. 3b). The electric field at that time is generally larger than at 0900 GMT due to the changed boundary condition. The inner edges moved to about 7 earth radii from the earth, in the equatorial plane; given a longer growth phase, they would probably have moved to lower L shells, making the computed results agree better with electron data (See discussion in section I-D).

The onset of the substorm resulted, in the program, from changes in three major input parameters. First, our substorm current loop (discussed in section I-B) was turned on to reach a peak value of 2×10^6 A at 1040 GMT (peak of substorm). Second, the conductivity jumps over one time step from its quiet time values to the values derived from the 1000 pass of S3-2. For later times we interpolate linearly between these values and the ones derived from the 1147 pass. Third, the polar-cap potential drop continues to increase to the peak value of 80 kV at 1040.

Figure 3c gives the potential distribution and plasma boundaries at 1040. By now we can see a clear tendency of the high-energy ions to penetrate best at dusk where they are inside of the zero-temperature particles by ∿ 2 R_E and the electrons are trailing by 4 R_E. The particles come in as close as ∿ 6.5 R_E geocentric distance in the equatorial plane, and are still drifting in.

At 1300 (figure 3 d) we are well into the recovery phase. By now the substorm loop is down to half its peak strength, and so are the conductivities in the night side ionosphere. The potential electric field is much better shielded and the plasma has moved in even further (as close as 5 R_E at dawn). Figure 4

shows the same potential and plasma configuration as viewed from above the north-polar ionosphere. Shielding is obvious equatorward of the equatorward edge of the plasma-sheet. The innermost circle (hidden among the equipotentials) is our boundary curve I, which maps to the polar-cap boundary.

Figure 5 shows plots of lines of constant $V-V_{corotation}+\lambda(\int \frac{ds}{B})^{-2/3}$ for high energy ions (roughly 50 keV). Thus these lines describe local trajectories of these ions as they drift around the Earth. The inner edge of the plasma sheet for this type of ions is also plotted. It is clear that these particles would have formed a complete or nearly complete ring, corresponding to a recovery time ring current. They did not, however, do this, because our numerical procedure does not allow an inner edge to cross local noon twice. This is seen even better in figure 6, where the inner edges are plotted for only three types of particles. At noon, the inner edges extend outside of our boundary curve I. The fact that the inner edges go outside curve I is physical, the exacted computed shape of the inner edges near noon is not physical.

D. Comparison with Data and Discussion

(i) Comparison with S3-2 Electric-Field Data

Only the polar-cap potential drop, computed by the integral of $E_{forward}$ all across the cap, was used as input to the program. The details of the observed electric field in the return-flow, sunward-convection region was then checked against the model-computed electric field. This comparison is presented in Figures 7a-7e.

In presenting these data and the corresponding theoretical curves, we should make the following qualifying remarks:
(i) The data from the AFGL electric-field detector on satellite S3-2, kindly provided by Dr. W. J. Burke and Dr. F.J. Rich is still in a somewhat preliminary form. The 1 October 1977 deadline for completion of work under contract F19628-77-C-0012 necessitated use of the data before all possible errors and noise could be eliminated. We are very grateful to Dr. Burke and Dr. Rich for supplying the data quickly for our use.
(ii) We tried to be totally honest in making this first simulation run. We therefore didn't adjust anything in the theoretical model to make it agree with the observations better. That is, we used certain observations as input in as straightforward a manner as possible, but we didn't adjust anything to improve the fit between model predictions and observations. For example, after we ran the growth-phase simulation, we realized that we probably underestimate the duration and/or strength of the growth phase. Nevertheless, we didn't rerun the growth phase. Figures 7a-7e represent a first try at a confrontation between observations and our theoretical model, with no fudging.
(iii) The theoretical electric-field plots presented in Figures 7a-7e were derived by taking symmetric differences of the values of the potential at our grid points, then interpolating in the two-dimensional grid to find electric fields at the satellite orbit. The electric fields are then corrected to satellite altitude assuming equipotential dipole magnetic field lines.

Comments on Comparisons of Data and Theory, Figure 7

1. Quiet times (Figs. 7a, 7b). We ran our model for two hours magnetosphere time with a 20 kV polar cap potential drop, to obtain a reasonable and relaxed initial condition. Our estimate of $\int E_{forward}\, d\ell$ for the phases shown in Figs. 7a and 7b, is $\sim$20 kV. Thus the result of that initial-condition run should, in principle, correspond to auroral-zone passes shown in Figures 7a and 7b, which occurred during quiet times before the injection event.

There is no significant correlation between theory and experiment in Figures 7a and 7b. We believe that this is because that particular S3-2 orbit just skimmed the polar cap, and that the data, taken during an extended quiet time, showed mostly weak, irregular and atypical electric fields.

2. North-south electric field during substorm. As indicated in Figures 7c-7e, agreement between theory and data is reasonably good.

3. Penetration of convection field equatorward of auroral-electron precipitation. In both the data and the model, the convection field penetrates substantially equatorward of the auroral electron precipitation during the injection event (Figures 7c-7e). This is particularly true in the dusk side, where most of the sunward convection occurs equatorward of the auroral zone (as defined by precipitating electrons). From a theoretical point of view, this results from the physics of the shielding process (Jaggi and Wolf 1973) and the assumption that electrons are lost by strong pitch-angle scattering. The shielding is primarily due to the protons, in this case where the electrons are assumed to be lost by strong pitch-angle scattering [Southwood and Wolf, 1977]; thus the shielding layer is the inner edge of the plasma-sheet ions. In the present model with strong electron pitch-angle scattering, the ions penetrate deeper into the magnetosphere than the electrons, because precipitation erodes the inner edge of the electron - plasma-sheet. In almost any convection model, positive ions tend to penetrate best on the dusk side, electrons best on the dawn side. (See review by Kivelson, 1977.)

4. Dawn- dusk asymmetry in the form of the meridional E.

Also noticeable in Figures 7c-7e is the fact that the theoretically predicted north-south electric field tends to decline something like a smooth power law on the dawn side, whereas on the dusk side the behavior is very unlike a power law. Starting

from the polar-cap boundary, the northward electric field first increases slightly with decreasing latitude, then drops sharply to a value near zero. We see two physical reasons for this asymmetry: (i) an effect of Hall conductivity and day-night asymmetry in the conductivities (see p. 4681 of Wolf (1970)); (ii) a substantial gap between the equatorward edge of the electrons and the shielding layer tends to result in large currents being carried across a low-conductivity region of the ionosphere; this tends to cause large electric fields just poleward of the shielding layer [Southwood and Wolf, 1977], particularly on the dusk side, where the gap between auroral electron precipitation and shielding layer is thicker. This dawn-dusk asymmetry is closely related to the phenomenon of rapid trough flow [Spiro et al., 1977, Smiddy et al., 1977] We shall have more to say about rapid trough flow, based on this simulation run, after we have had time for detailed study of the computed Birkeland-current distribution and the electric-field fine structure.

5. East-west electric fields. In one case (outbound part of Figure 7d), there is good agreement between theory and observations with regard to the east-west electric field. In all the other cases, the theoretically computed east-west electric field is substantially smaller, in absolute magnitude, than the observed field. As yet, we have no theoretical explanation for this discrepancy.

6. Location of polar-cap boundary. In the data plots of Figures 7a-7e, the polar-cap boundary is indicated by an "X". Specifically, the "X" marks the beginning of the sharp drop in the absolute magnitude of the meridional electric field, just equatorward of the equatorwardmost electric-field reversal. In essentially all cases, the observed polar cap (defined in this special way) was a few degrees wider than the model polar cap across which we applied the assumed potential drop (Figure 2B). This discrepancy also caused the model sunward-convection region not to extend to as low latitudes as the observations indicate.

(ii) Injection of Ring-Current Particles

In the model, the dawn-dusk potential electric field, of course, increases in time through the growth phase and the first 40 minutes after onset, tending to drift particles nearer the earth near local midnight. The turning on of the substorm current loop creates an additional westward electric field near midnight, and additional earthward drift there.

What energy ions would one expect to penetrate closest to the earth on the dusk side? There are two competing effects: (i) in a time-independent situation, the best penetrators are low-energy ions whose gradient-drift speed approximately balances corotation; high-energy ions penetrate much less well [see e.g., Chen, 1970]; (ii) the message that there was an injection near midnight propagates along the inner edge for particles of given energy at a speed equal to the particles' local drift speed; thus the message would propagate fastest for high-energy protons, and we might expect them to be the first to come in at some local times.

It isn't immediately obvious which effect should dominate. In all previous runs, in which we had always let the plasma sheet drift in gently, with no induction electric field, effect (i) always dominated and low-energy protons penetrated best at nearly all local times.

In this first run aimed at simulating a substorm, effect (ii) turned out to be dominant, and high-energy protons penetrated best on the dusk side. Figure 8 shows what particle detectors sitting at a geocentric distance of $7R_E$ near local dusk would have seen during the 19 September event, according to our computer model. At first, no particles would have been seen. Slightly more than 30 minutes past onset, the detector would see 53 keV ions (the highest-energy ions we followed). As time passed, the detector would have seen a wider and wider range of energies. Three hours after onset, it would be seeing 5 KeV- 53 KeV ions. This sort of behavior is what has been observed many times during substorms by McIlwain and collaborators [see, e.g., DeForest and McIlwain,

1971] on geosynchronous satellites and also by Konradi et al (1975) on satellite S^3. Encouragingly, this basic feature came out automatically out of our first effort at simulating a substorm. Roederer and Hones (1974) obtained similar results several years ago using an ad hoc substorm potential electric field (time-independent dawn-dusk electric field + time dependent electric field that included a large westward field near midnight). We have now found that this basic energy-dispersion result comes out of the calculation when we use a realistic induction electric field and a self-consistently calculated potential electric field.

Unfortunately, the ATS-6 satellite was near magnetic noon for the 19 September event, and although we have spectrograms for the event (provided by Dr. D. L. Reasoner), it isn't clear yet how useful these will be. Also unfortunately, the program didn't keep track of the absolute inner edge of the electron plasma sheet-- only the edge as represented by 25% and 75% precipitation, assuming strong pitch-angle scattering. These 25% and 75% precipitated boundaries never penetrate very close to the earth because of the rapid loss assumed. In future runs we can easily keep track of the absolute inner edge and calculate electron energy-vs- arrival time, curves analagous to Figure 8.

Comparing Figure 6, which shows the position of the boundary of the high-energy protons at 1300 UT, with Figure 5, which shows their instantaneous drift paths, it is clear that these particles are going to form something close to a complete ring. Thus we have modeled the beginning of the injection of a real ring current. Unfortunately our present way of treating the plasma-sheet boundary does not allow the inner edge for any component to cross a given local-time line more than once. Consequently, the numerical procedure is artificially preventing the enrgetic-ion boundaries from drifting westward past local moon. We stopped the program at 1300 UT, because this problem was becoming critical. Nevertheless, it is clear that the system is trying to form a complete or nearly complete ring.

II. SECOND OBJECTIVE: INITIAL COMPUTER MODEL FOR COLD PLASMA FLOW ALONG FIELD LINES

The objective of this work is to understand spatial and temporal variations in the properties of cold plasma in the topside ionosphere and plasmasphere. After some study of the problem, we have formulated a simple initial approach to this complex problem, namely, we programed the computer to keep detailed track of the time history of the motions of an arbitrary flux tube during a simulated event. Combined with topside-ionosphere data from the period of the simulated event, results of our program should provide interpretations of some of the observed structures.

We have completed a draft program to do the calculation described above. Namely, the program will take a set of flux-tube positions at some t and integrate their $\underline{E} \times \underline{B}$ drifts backwards in time, using the computed potential distributions that have been recorded on the computer's disk, at 10-minute intervals during the simulated event. The program will determine which flux tubes, at the end of the event, have recently come in from the magnetotail and therefore have relatively low plasma densities. It will thus predict the plasmapause location and light ion trough shapes as functions of time through the event, including any associated final structure; the procedure is applicable to either the topside ionosphere of the equatorial plane.

For the 19 September event there were, as far as we know, no satellites out in the magnetosphere measuring cold-plasma densities. It is not clear yet whether useable cold-plasma results will be obtained from S3-2 or any other polar orbiter. In any case, we intend, in the coming year, to apply our flux-tube tracing program to the 19 September 1976 event and other events and calculate plasmapause and trough shapes, with associated fine structure.

III. THIRD OBJECTIVE: CONDUCTIVITY MODEL

A conductivity model is an important integral part of our event simulation. The conductivity model serves as input to the equation for conservation of ionospheric current (equation 2 in section I-B), which we solve numerically to find the potential distribution in the ionosphere.

In general, one may think of the height-integrated conductivity as consisting of three terms. The first is the conductivity due to the solar radiation and the photoionization that results. This term appears in our program as time independent and is a function of solar-zenith angle and local time only. The second is the low-latitude nightside conductivity, which is physically complicated but has been repeatedly measured [Rowe and Mathews, 1973]; it also appears in our program as a time-independent term. The third term is the auroral-enhancement term, representing the increased electron density due to precipitation of kilovolt electrons at auroral latitudes. This term depends in a complicated way on universal time, latitude and local time.

To estimate the spatial dependence of the auroral enhancement in an accurate way, for the whole auroral zone, one would need global measurements of electron density or global measurements of the flux of auroral electrons incident on the ionosphere. Such measurements are, of course, not available, and one must approximate or extrapolate available data.

Use of S3-2 Electron Data

The primary method we have used to estimate height-integrated conductivities for the 19 September event involves an empirical formula that we derived, relating height-integrated Pedersen and Hall conductivities to electron energy flux and mean electron energy. M. H. Rees and his collaborators [Rees and Jones, 1973, and Rees, private communication] have calculated electron-density profiles in the nighttime-auroral ionosphere for various energy fluxes and mean energies, and for certain as-

sumed neutral-atmosphere models. Using standard formulas for Pedersen and Hall conductivities, formulas based on momentum equations for ions and electrons [Rishbeth and Garriott, 1969], we deduced height profiles of Hall and Pederson conductivities for three of Rees' models. We then numerically integrated these over height and fitted the results to simple power laws, with the following results:

$$\Delta\Sigma_p = (5.2 \text{ mhos}) \left[\frac{\text{Energy flux}}{\text{erg/(cm}^2\text{sec)}} \right]^{\frac{1}{2}} \qquad (3)$$

$$\frac{\Delta\Sigma_H}{\Delta\Sigma_p} = 0.55 \left[\frac{\text{Average electron energy}}{1 \text{ KeV}} \right]^{0.6} \qquad (4)$$

Therefore, once we determined the electron flux and average energy from S3-2 data, we derived the corresponding height-integrated conductivities. For our substorm simulation we used electron flux measurements from four passes on 19 September 1976: 0400, 1000, 1140 and 1500 GMT. For every pass we determined the flux as a function of invariant latitude.

The resulting height-integrated Pedersen and Hall conductivities at local midnight are plotted in Figure 9 as a function of latitude at 0900,1000 (onset) and 1200 GMT (near peak). The following assumptions were used: a) conductivity was kept constant at its quiet-time value until 1000 (onset). We simulated the onset by a discontinuous jump in conductivities. Thereafter, we linearly interpolated in time to the next data point (at $\sim$ 1140). From 1140 on, we simulated the recovery phase by a gradual decline to the final quiet-time value (1500) over a period of 3 hours. b) Since our numerical procedure for solving equation 2 has trouble dealing with a sharp order of magnitude jump in conductivity at the equatorward edge of the auroral zone, we applied a smoothing function to that equatorward edge, restraining the jump to be a factor of $\lesssim$ 3 over a grid spacing.

c) For simplicity, the local-time dependence of the auroral conductivity enhancements was assumed to be described by a simple analytic formula:

$$\Delta\Sigma(\lambda,\Psi) = \Delta\Sigma(\lambda,0)\ [0.75 - 0.25 \cos\ (\frac{\pi(\Psi+12)}{24})], \quad (5)$$

where Ψ= magnetic local time in hours and λ= invariant latitude.

Use of DMSP Photos

Originally, we planned on estimating electron fluxes directly from DMSP photos. We did find that brightness of the auroral images correlate with the electron flux into the ionosphere. However, we encountered some major difficulties in applying this procedure to the event of 19 September 1976. First, the period of the year (near equinox) does not favor the DMSP's (because of the polar cap and auroral zone being partly in sunlight). Second, it is hard, technically, to measure quantitatively the changes in brightness all the more so since the copies we had, in many cases, did not contain all the features of the original photographs. On the plus side, the DMSP photographs did help us determine the equatorward edge of the diffuse aurora and also provided a crude check of the results obtained by our primary method.

Our rough method of calibrating the DMSP photographs is based on comparison of a few DMSP photographs covering the area near the Chatanika radar with height-integrated conductivities measured approximately simultaneously by the radar, which was operated in an L-scan mode. (The copies of DMSP photos were provided by the World Data Center. Data from the Chatanika radar were kindly provided by Dr. R. R. Vondrak of Stanford Research Institute, and we are immensely grateful to him for quickly analyzing the radar data that we needed.) Our calibration efforts verified the correlation between bright features and high-conductivity regions. Using this rough calibration, we estimated Hall conductivities from several DMSP photos during the substorms. The comparison between these values and Hall conductivities obtained by our primary method was reasonable (for bright features, the values agree to within a factor of 2).

We also used the photographs from the 19 September substorms to remove an amgiguity in the interpreting the S3-2 electron fluxes. Namely, we had, at the time, no pitch-angle data available for the electron fluxes and consequently had trouble distinguishing trapped electrons from precipitating electrons. We used the location of the lower edge of the diffuse aurora to decide between two possible boundary locations suggested by the S3-2 data. We now have in hand better integrated electron data with pitch angle information from S3-2 (provided by Dr. David A. Hardy). This should improve our second attempt considerably.

The lower edge found in this way agrees nicely with Winningham's observation of the expansive phase (Winningham et al., 1975).

IMPLICATIONS FOR FUTURE WORK

We have just completed our basic first simulation run, and the results need much more analysis. Presented below are some tentative ideas for further work.

Further studies of the results of the first run:

1. Compute fine-structure of electric field and check for prediction of rapid trough flow.
2. Compute distribution of Birkeland current at various times through the event and compare with TRIAD data, and with S3-2 data, when it becomes available.
3. Compute shapes of plasmapause and light-ion trough at various times through the event, and compare with polar-orbiter data if it becomes available.
4. Compute ground magnetic variations from the model current system and compare with ground magnetograms.

Changes in boundary conditions-for reruns of the simulation of the 19 September event:

1. Apply specified polar-cap potential across a more accurate polar cap.
2. Check the effect of a longer assumed growth phase.
3. Assume electrons precipitate more slowly than implied by the original assumption of strong pitch-angle scattering.
4. Check the effect of varying the conductivity model.
5. Follow the motion of the absolute inner edge of the electron plasma sheet in order to check the predicted arrival-times-vs.- energy relation against what McIlwain normally observes. It will be interesting to see if our self-consistent theoretical electric-field model can, with detailed analysis, do as good a job of fitting observations as the semiempirical electric field models used by McIlwain (1974), Roederer and Hones (1974) and Konradi et al. (1975).
6. Run our program without the polar substorm current loop to see if we get McIlwain-type energy dispersions without an induction electric field.

The following list gives the most urgently needed improvements in our basic program:

1. Use the Olson-Pfitzer full numerical model rather than the analytic model.
2. Rewrite the subroutine that arranges for automatic pressure balance near the inner edge of the plasma sheet.
3. Revise the method of following boundary motions to allow the inner edge to cross a given local time more than once (to allow us to follow formation of a complete ring current).
4. Include a reasonable empirical model of neutral winds in the ionosphere.
5. Include an empirical model of field-aligned potential drop, estimating the drop on the basis of electron spectra and/or DMSP photos.
6. Define a method for using DMSP electron data to calibrate the corresponding photo, for the purpose of a quantitative global estimate of the distribution of auroral height-integrated conductivities. Dr. Hardy has begun a study of cross-correlating DMSP and S3-2 data, which may be helpful to us in this regard.

FIGURE CAPTIONS

Figure 1. Diagram of the logic of our program. The diagram is a revision of one given by Vasyliunas (1970). Arrows indicate flow of information in the program. Dashed lines indicate features that we are trying to incorporate in the program, but we did not include in the first simulation run. The program cycles through the entire main loop (including all the rectangular boxes) every time step Δt (approximately every 30 seconds). Time advances on the upper right side of the pentagon, when the hot-particles are allowed to drift for a time Δt. The basic equations that the computer uses or solves are described briefly by words or symbols next to the logic-flow lines.

Figure 2. a) Fort Churchill magnetogram of Sept. 19, 1976. The substorm that was simulated had its onset at 1000 GMT and peaked at about 1040. The system slowly recovered from these till 1500. B_{north} is plotted upside down (at 1040 B is most negative). The peak value corresponds to a dip of $\sim$ 520 γ. A small disturbance is seen around 0600 GMT.
b) Observed polar cap potential drop. The data points represent the average potential drop $\int E dl$ across the polar cap. data point is defined by data from one north polar-cap or one south polar-cap crossing of satellite S3-2. The size of the boxes correspond to the error bars. The solid line represents our choice for the cross-polar-cap potential drop. (Given a second chance we, will, likely, extend the duration of the growth phase, presently confined to the period 0900 to 0100 GMT.)

Figure 3. Potential contours computed by the theoretical model for various phases of the substorm. Figures a-d present electric potential in the equatorial plane at the beginning of the growth phase, onset, peak, and recovery of the substorm respectively. The time is Universal Time. The distance scale is in earth radii away from the earth. The view is from above the equatorial plane (sun to the left). The curves plotted are equipotentials spaced 8 kV apart. The outermost closed curve is the mapping of our boundary (equatorward of the polar cap).

The other 3 contours (in the key) represent the inner edge of 3 of the 21 different species that we keep track of.

Figure 4. Equipotential lines in the ionosphere. The view is from above the north pole. The spacing between two successive lines is 8 kV. The inner circle is our boundary curve I and is offset 2° toward midnight. Also plotted are locations of 3 of the 21 types of particles and energies we model.

Figure 5. High energy ions (∿50 keV) local trajectories. The plot is an equatorial-plane view for the late recovery phase - 3 hours after onset.

Figure 6. Inner edge of 3 types of particles: ∿ 2 keV electrons, zero temperature and ∿50 keV ions. The outer circle is the mapping of curve I of figure 4.

Figure 7. Comparison of observed and predicted electric fields, for five different passes of satellite S3-2 through the auroral zones and polar caps. E_X and E_Y represent northward and eastward electric fields, in millivolts per meter. The data are plotted as thin solid curves below the "polar cap"; as dotted curves in the polar cap. Boundaries of the polar cap are indicated with X's. An upward-pointing bracket is used when a data gap prevented observational determination of the boundary. A bar with an "e" above it indicates electron precipitation. The thick black curves are theoretical curves, computed for the actual satellite trajectory. The X's on the theoretical curves represent the assumed polar-cap boundary. The legend at the bottom gives Greenwich Mean Time in seconds and also in hours: minutes: seconds, satellite altitude in kilometers, magnetic local time, and invariant latitude.

Figure 8. Ion arrival times at $r=7R_E$, MLT=1820. The solid curve shows the arrival time for particles of various energies at geocentric distance=$7R_E$, Magnetic Local Time=1820. The dotted line shows what the arrival times would be for ions of

various energies that gradient drift in the equatorial plane of a dipole magnetic field, with no electric field. The X's represent energies of the ions that we follow in detail. Specifically, an "X" means that the inner edge for that energy is earthward of $r=7R_E$.

Figure 9. Nighttime Pedersen and Hall conductivities. The conductivities (in mhos.) are plotted as a function of invariant latitude in the Earth's ionosphere. The three Pedersen-Hall pairs correspond to three different times: Quiet time, onset and 1100 UT (conductivity peak according to the data). The vertical times mark the location of polar-cap boundary and the equatorward edge of the electron-plasma sheet.

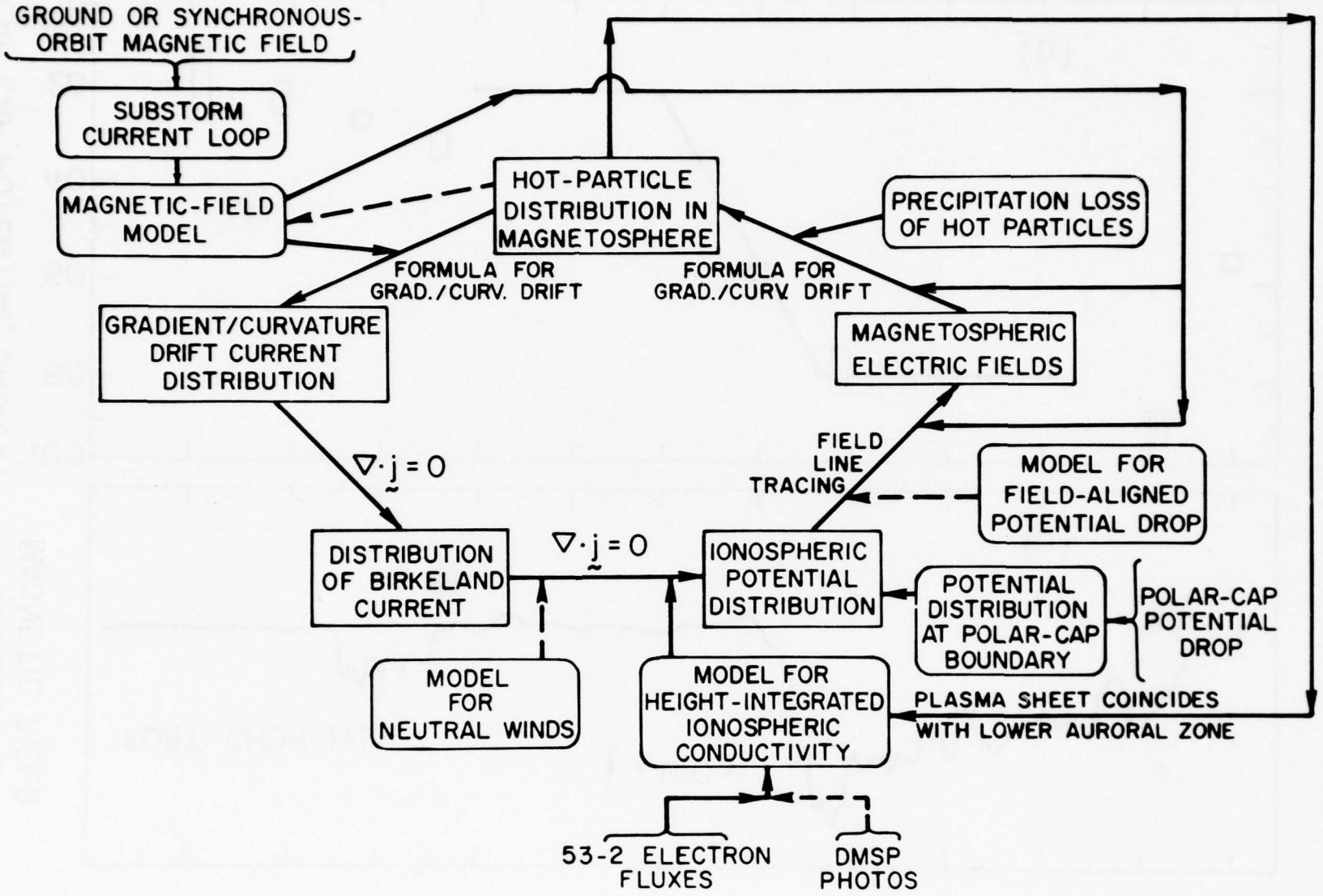
GROUND OR SYNCHRONOUS-ORBIT MAGNETIC FIELD
SUBSTORM CURRENT LOOP
MAGNETIC-FIELD MODEL
HOT-PARTICLE DISTRIBUTION IN MAGNETOSPHERE
PRECIPITATION LOSS OF HOT PARTICLES
FORMULA FOR GRAD./CURV. DRIFT
FORMULA FOR GRAD./CURV. DRIFT
GRADIENT/CURVATURE DRIFT CURRENT DISTRIBUTION
MAGNETOSPHERIC ELECTRIC FIELDS
$\nabla \cdot \underset{\sim}{j} = 0$
FIELD LINE TRACING
MODEL FOR FIELD-ALIGNED POTENTIAL DROP
DISTRIBUTION OF BIRKELAND CURRENT
$\nabla \cdot \underset{\sim}{j} = 0$
IONOSPHERIC POTENTIAL DISTRIBUTION
POTENTIAL DISTRIBUTION AT POLAR-CAP BOUNDARY
POLAR-CAP POTENTIAL DROP
MODEL FOR NEUTRAL WINDS
MODEL FOR HEIGHT-INTEGRATED IONOSPHERIC CONDUCTIVITY
PLASMA SHEET COINCIDES WITH LOWER AURORAL ZONE
53-2 ELECTRON FLUXES
DMSP PHOTOS

Figure 1

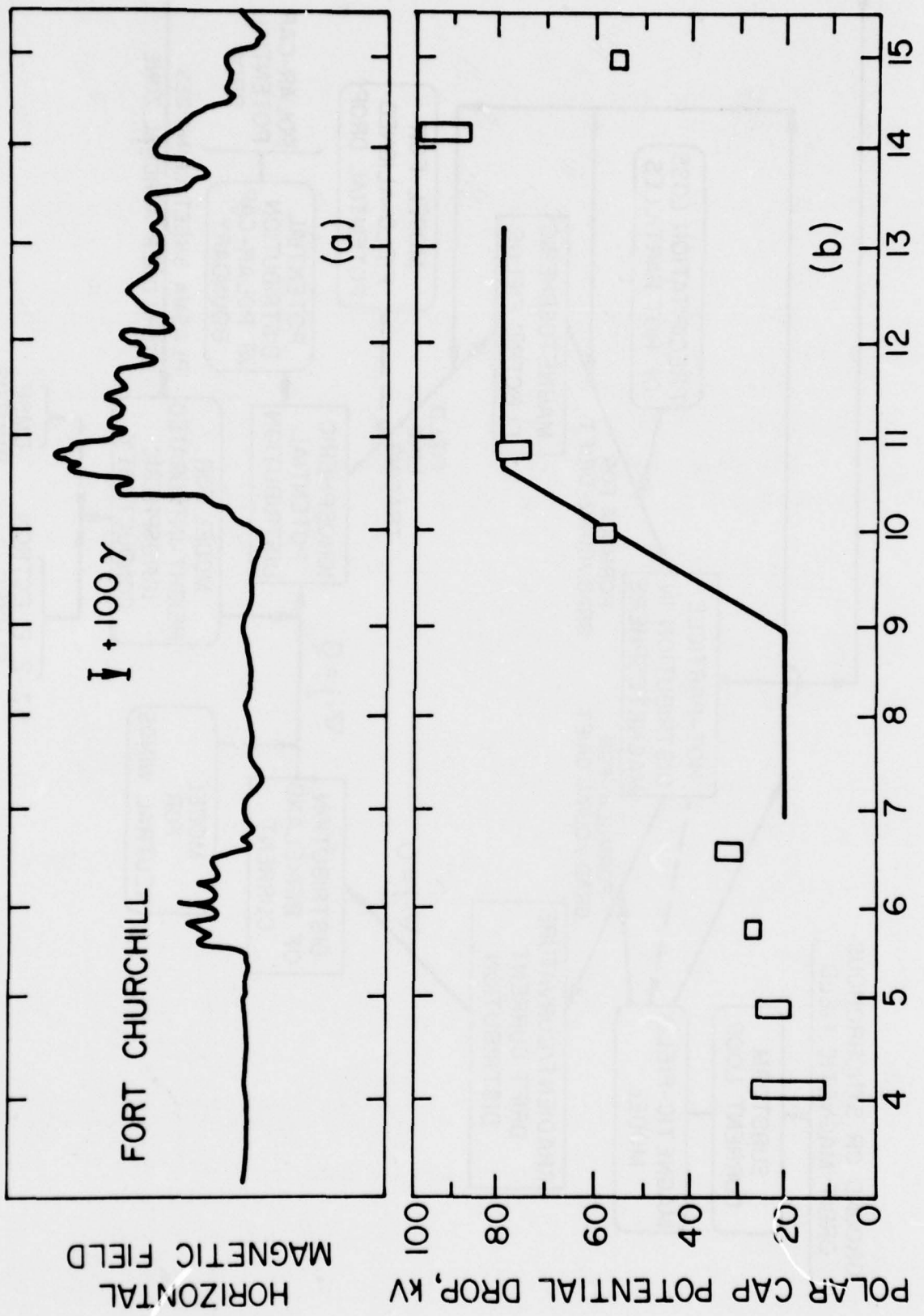
HORIZONTAL MAGNETIC FIELD
FORT CHURCHILL
+100γ
(a)
POLAR CAP POTENTIAL DROP, kV
0
20
40
60
80
100
4
5
6
7
8
9
10
11
12
13
14
15
UT
(b)

Figure 2

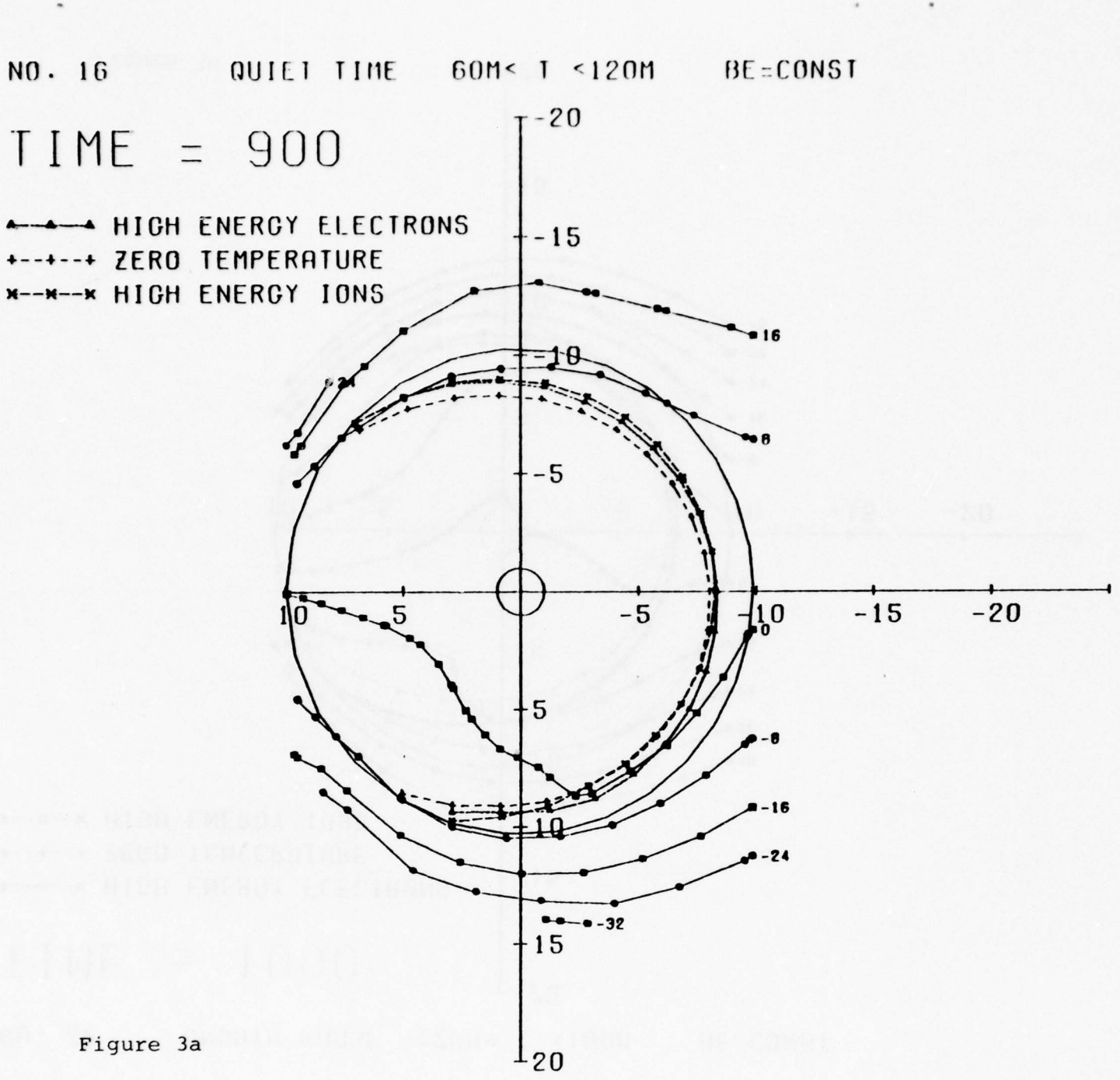
NO. 16 QUIET TIME 60M< T <120M BE=CONST
TIME = 900
HIGH ENERGY ELECTRONS
ZERO TEMPERATURE
HIGH ENERGY IONS
-20
-15
-10
-5
5
10
15
20
16
8
0
-8
-16
-24
-32

Figure 3a

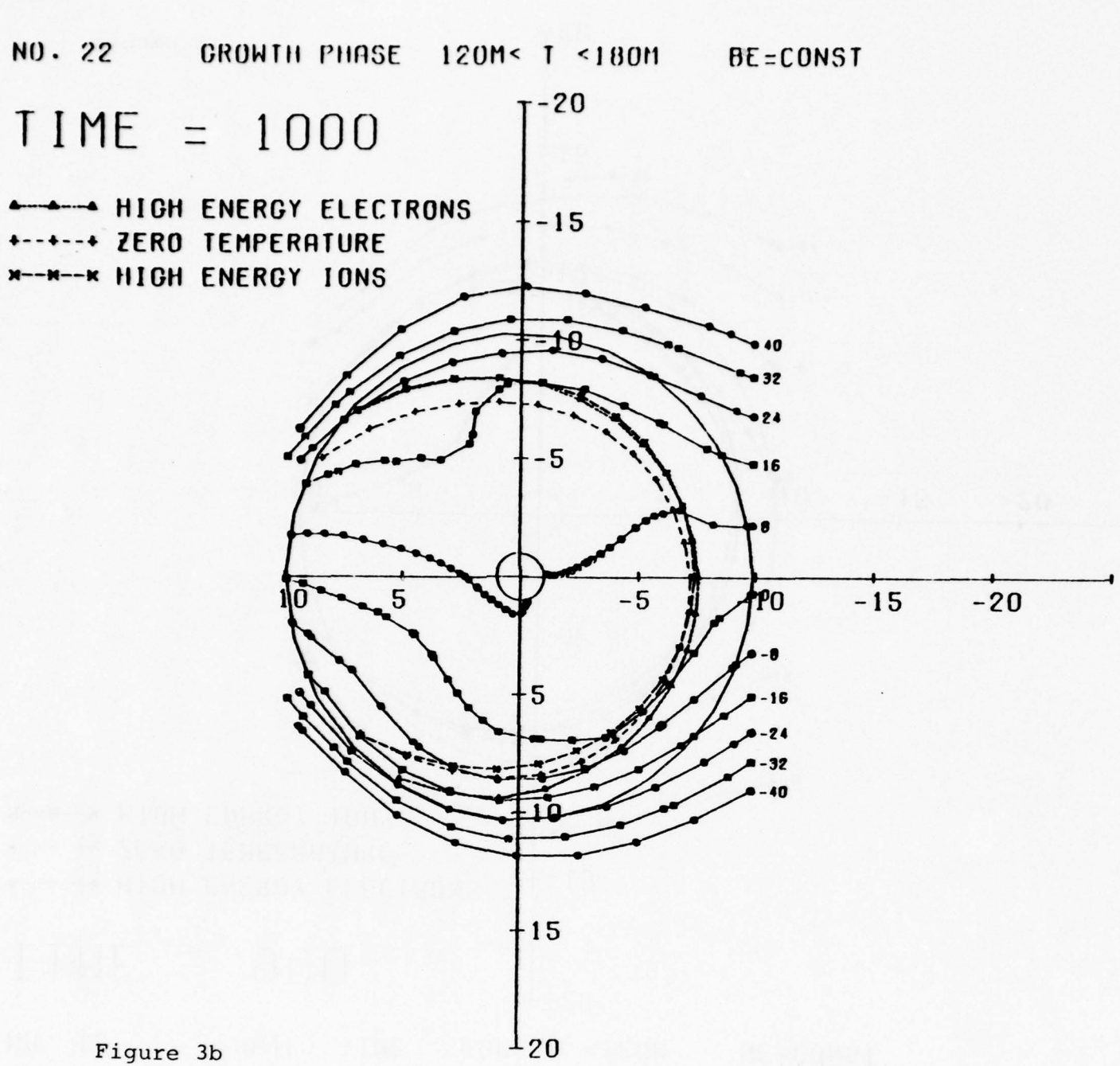
NO. 22 GROWTH PHASE 120M< T <180M BE=CONST
TIME = 1000
HIGH ENERGY ELECTRONS
ZERO TEMPERATURE
HIGH ENERGY IONS
-20
-15
-10
-5
5
10
15
20
40
32
24
16
8
-8
-16
-24
-32
-40

Figure 3b

NO. 23 ONSET & 1ST PHASE OF STORM 180M< T <220M

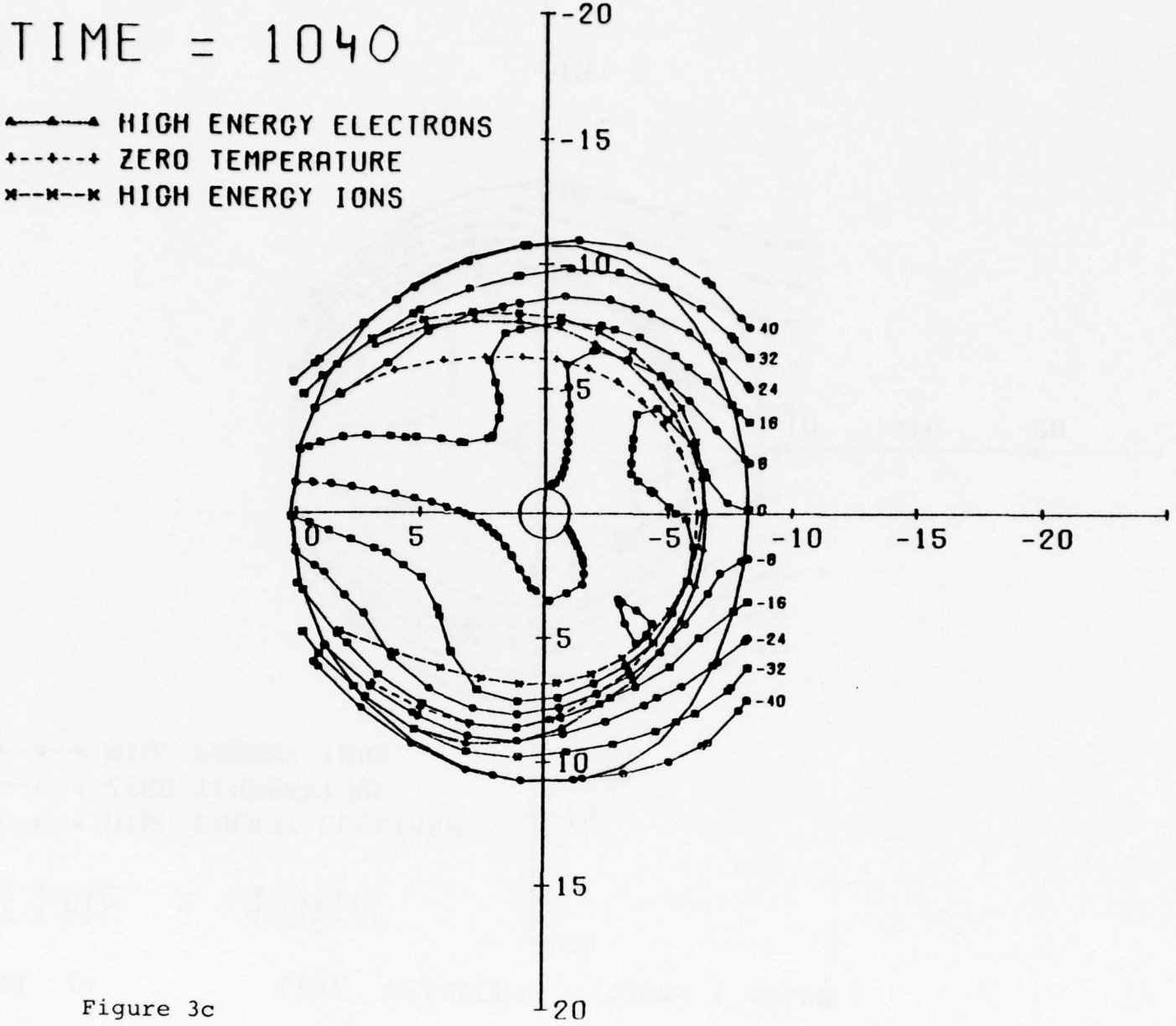

Figure 3c

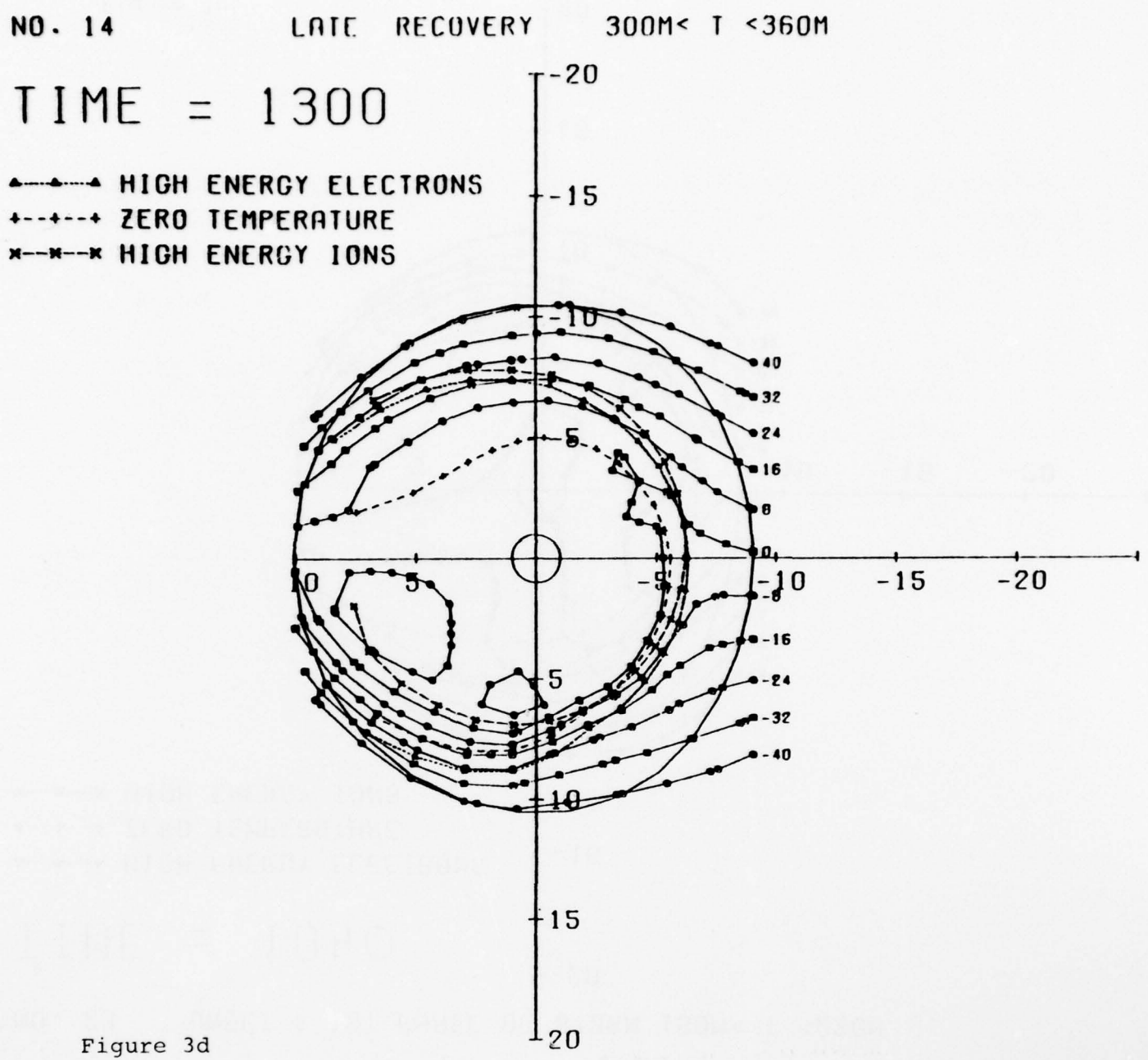
NO. 14 LATE RECOVERY 300M< T <360M
TIME = 1300
HIGH ENERGY ELECTRONS
ZERO TEMPERATURE
HIGH ENERGY IONS
-20
-15
-10
-5
0
5
10
15
20
40
32
24
16
8
0
-8
-16
-24
-32
-40

Figure 3d

NO. 14 LATE RECOVERY 300M< T <360M

TIME = 1300

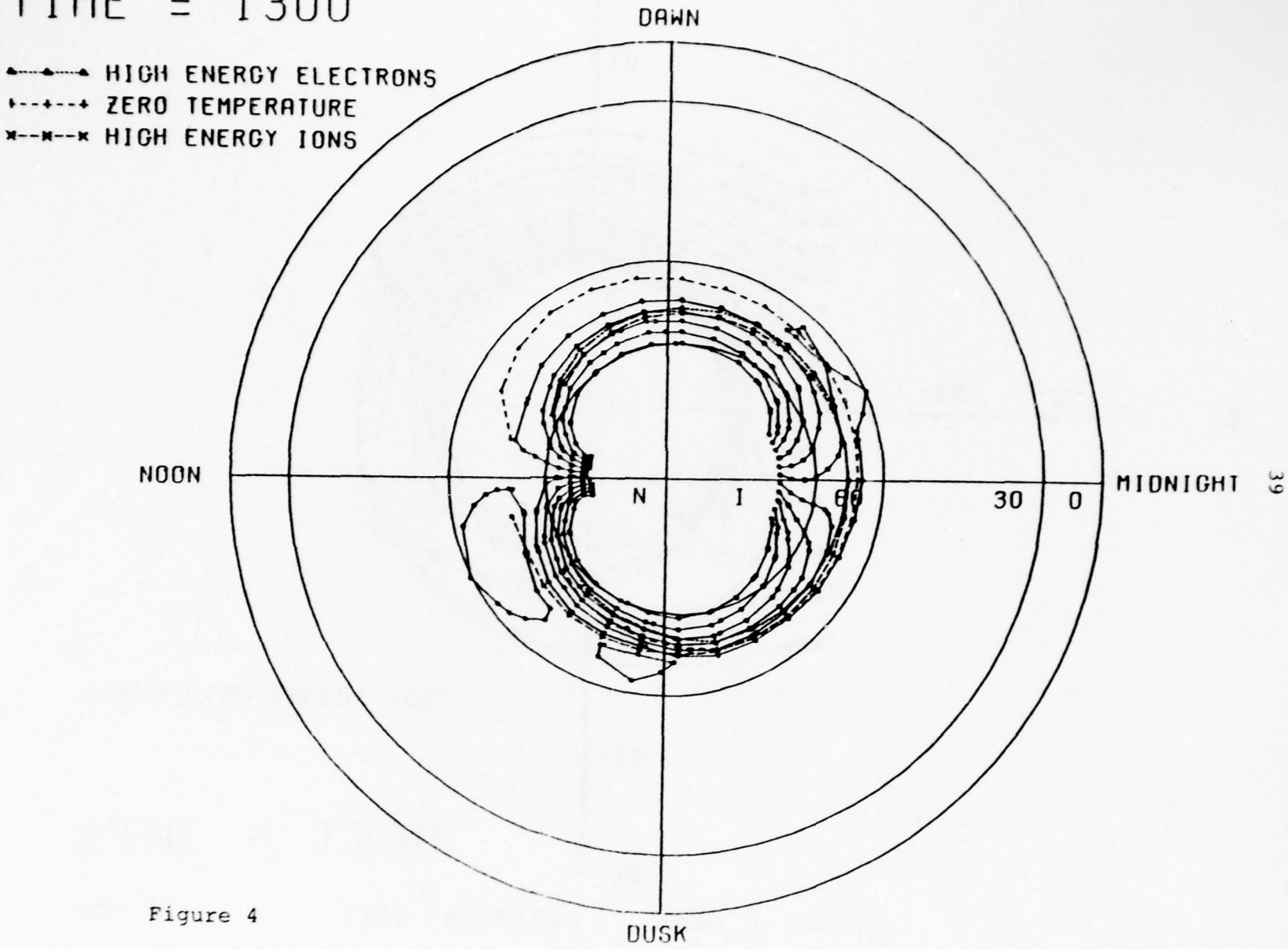

Figure 4

NO. 14 LATE RECOVERY 300M< T <360M

TIME = 1300

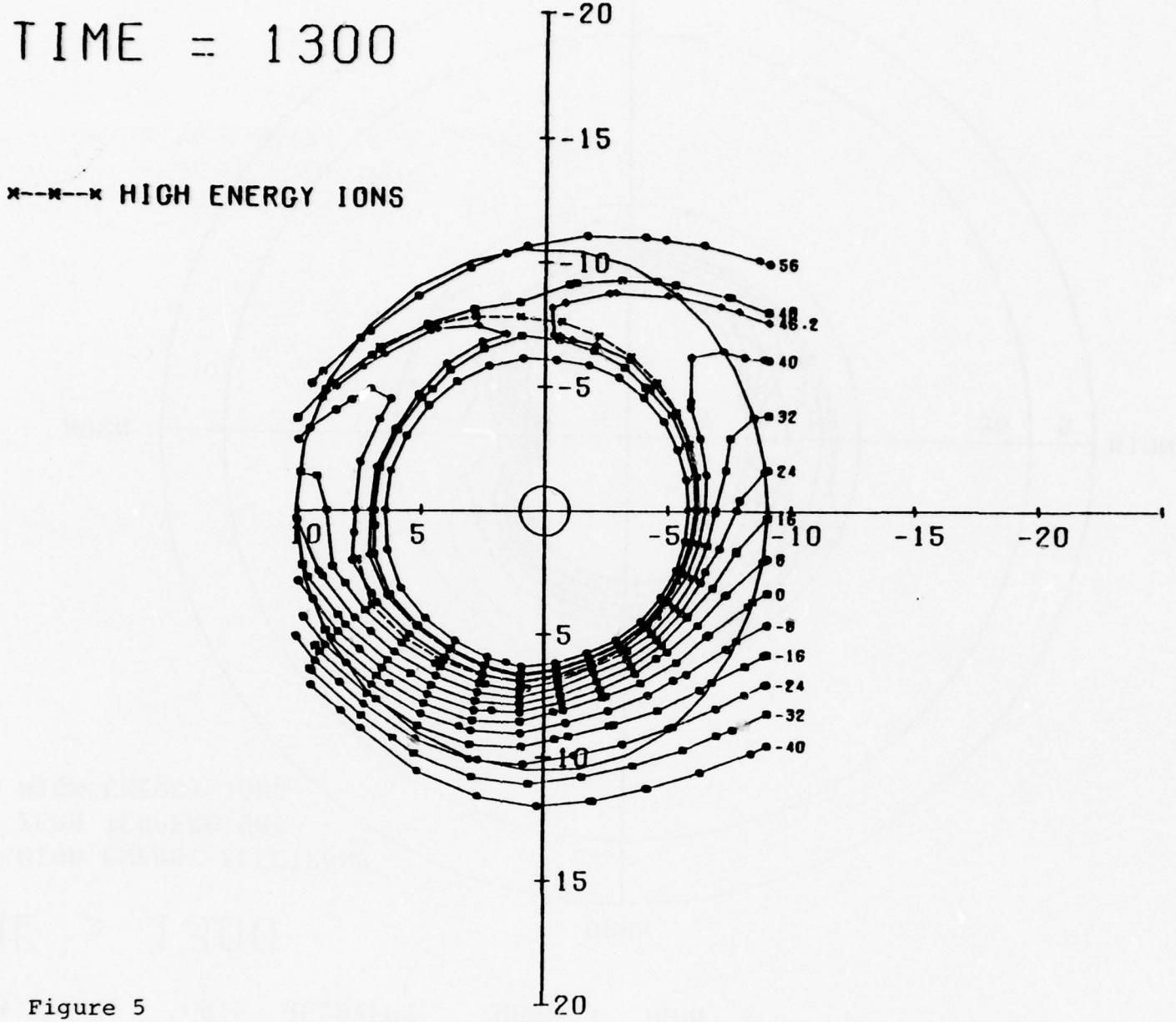

Figure 5

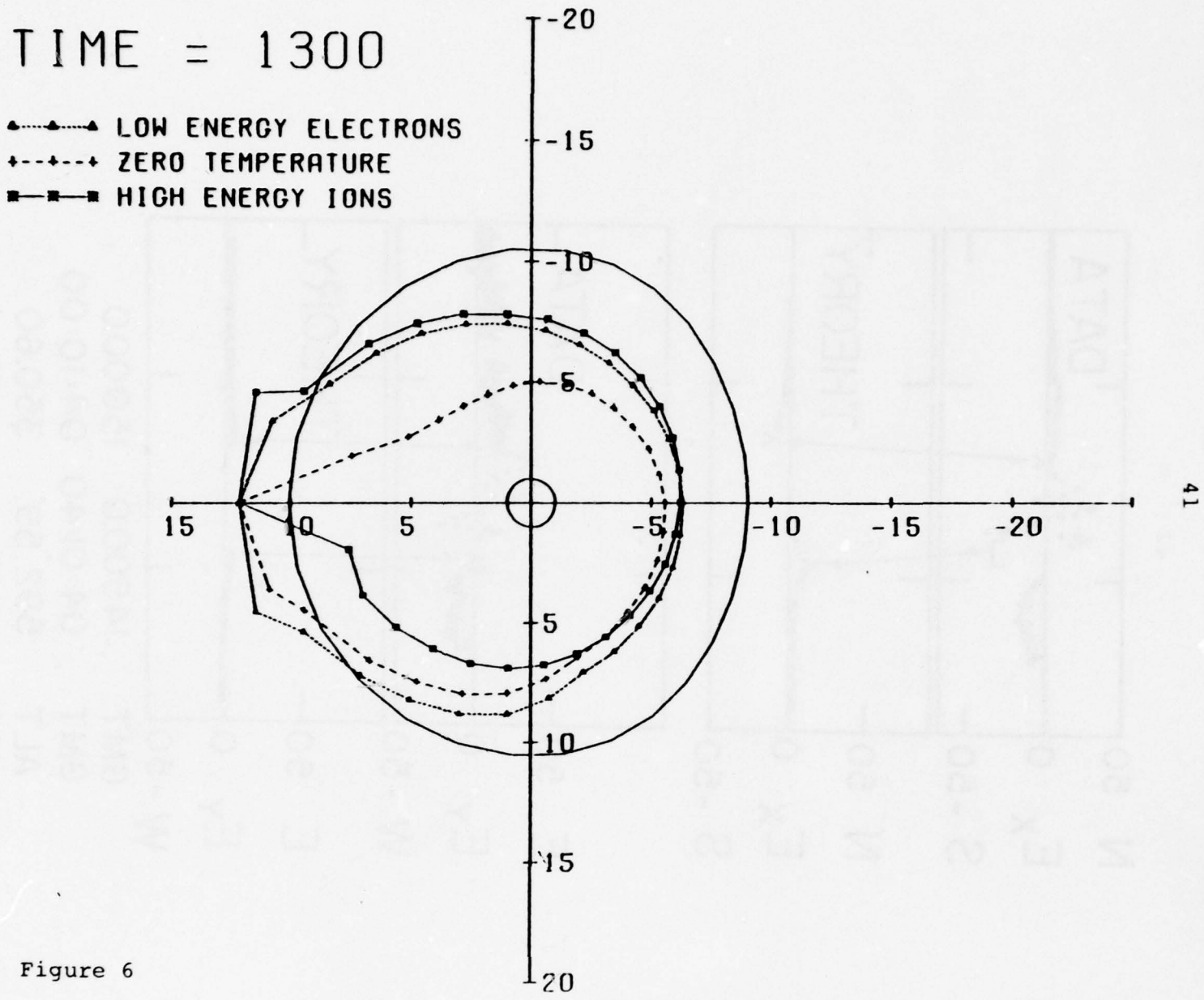
NO. 14
LATE RECOVERY
300M< T <360M
TIME = 1300
LOW ENERGY ELECTRONS
ZERO TEMPERATURE
HIGH ENERGY IONS
-20
-15
-10
-5
15
10
5
-5
-10
-15
-20
5
10
15
20

Figure 6

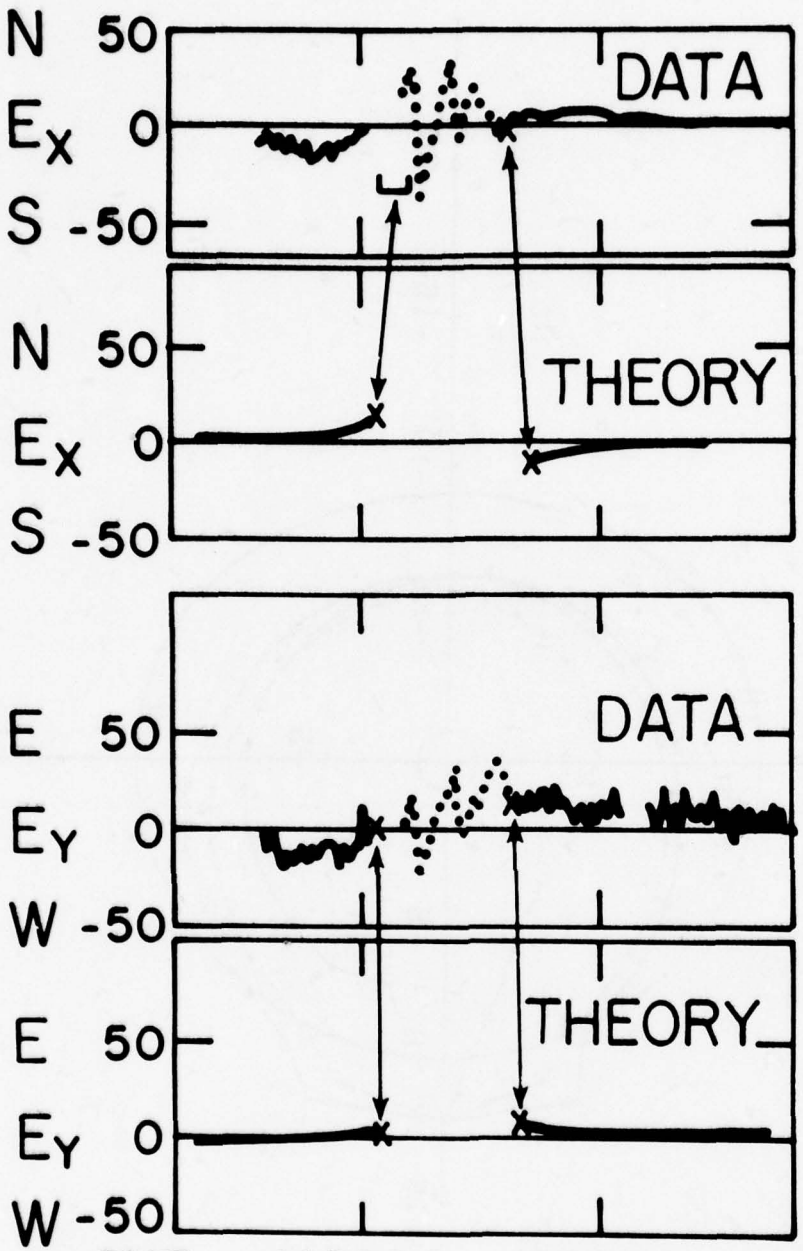

ORBIT 4078 NORTH

Figure 7a

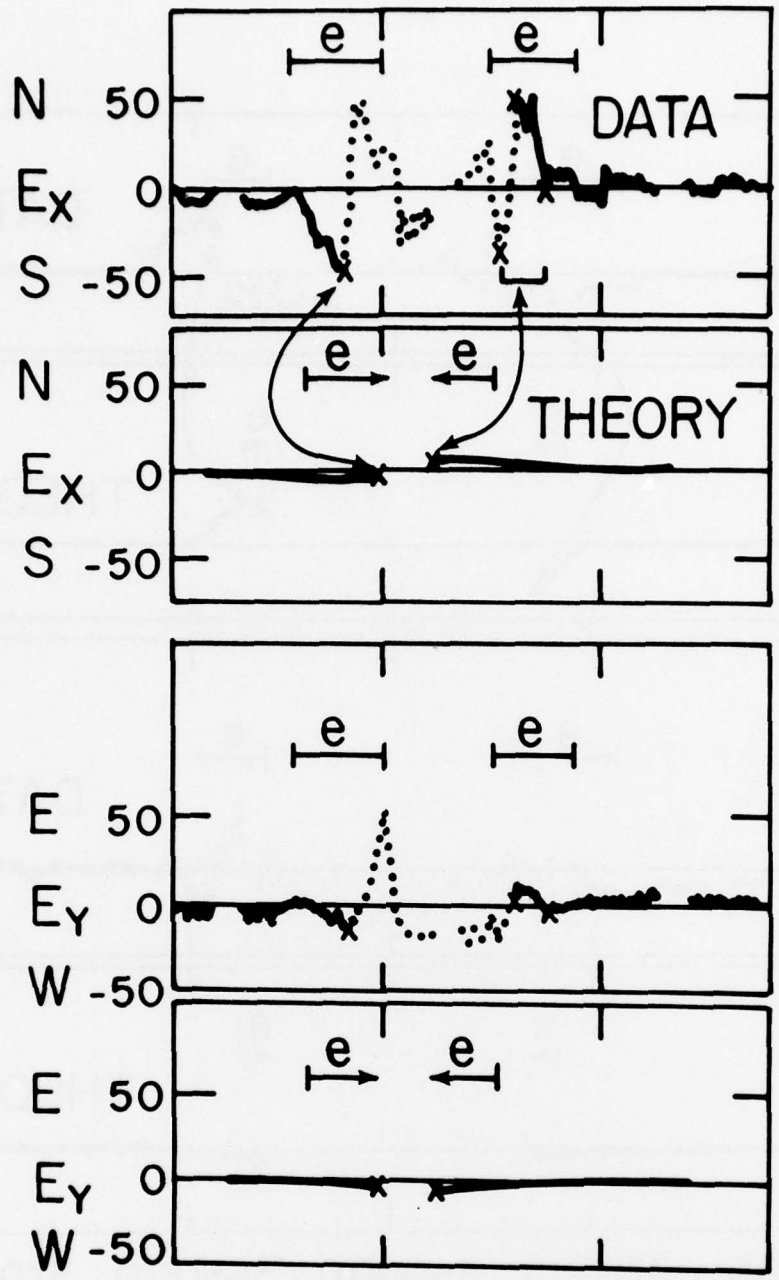

GMT	17000.0	17500.0	18000.0
GMT	04:43:20	04:51:40	05:00:00
ALT	825.04	1106.91	1307.42
MLT		1.52	21.82
ILAT	60.30	70.11	61.33

ORBIT 4078 SOUTH

Figure 7b

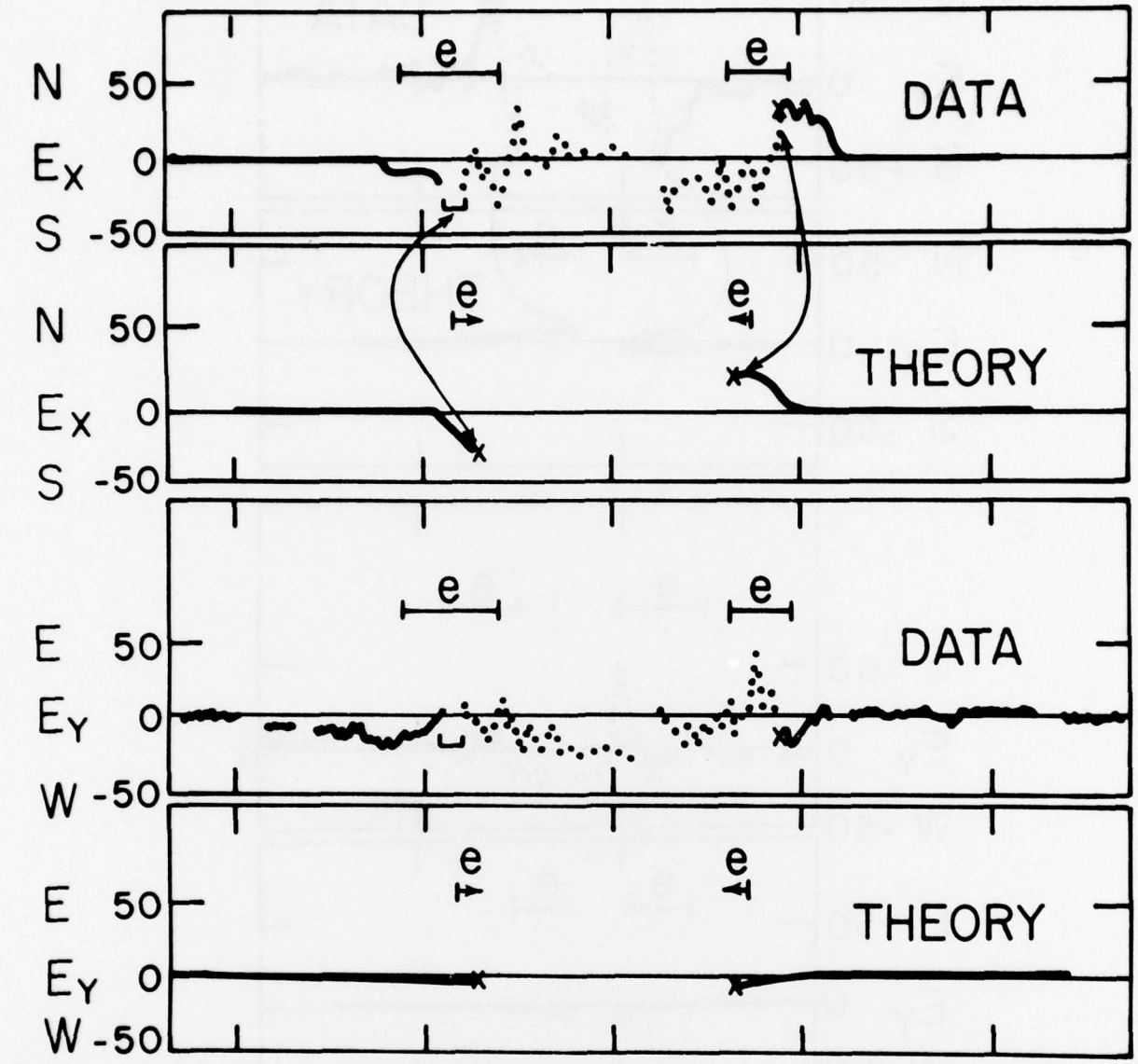

GMT	35000.0	35500.0	36000.0	36500.0	37000.0
GMT	09:43:20	09:51:40	10:00:00	10:08:20	10:16:40
ALT	726.43	1024.95	1258.16	1374.69	1363.90
MLT	6.35	5.85		19.97	
ILAT	41.67	64.66	81.52	62.55	38.96

ORBIT 4079A SOUTH

Figure 7c

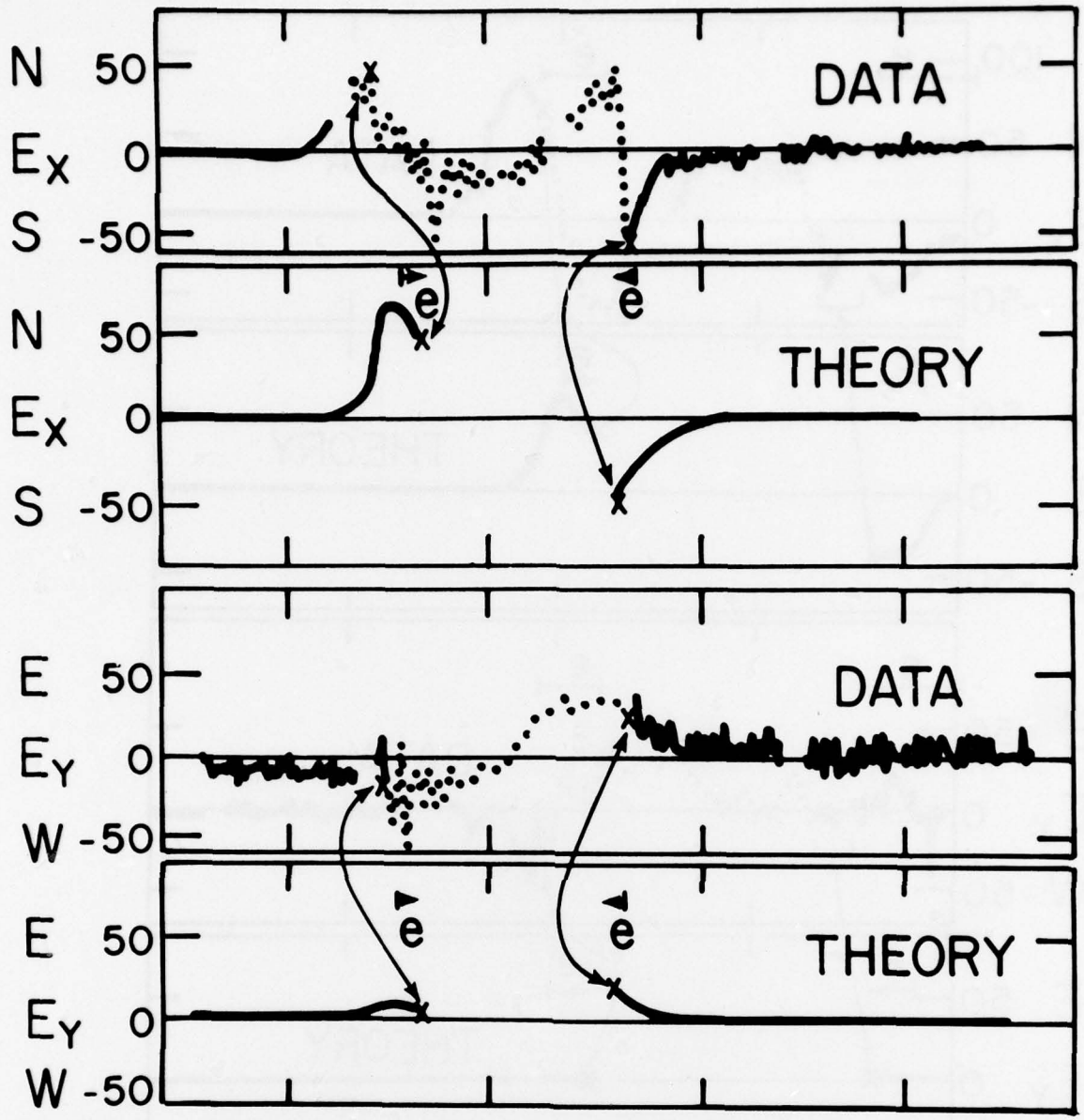

GMT	38500.0	39000.0	39500.0	40000.0
GMT	10:41:40	10:50:00	10:58:20	11:08:40
ALT	713.65	442.39	264.39	249.82
MLT	18.44	15.09	8.64	7.50
ILAT	54.48	79.32	62.76	34.32

ORBIT 4079A NORTH

Figure 7d

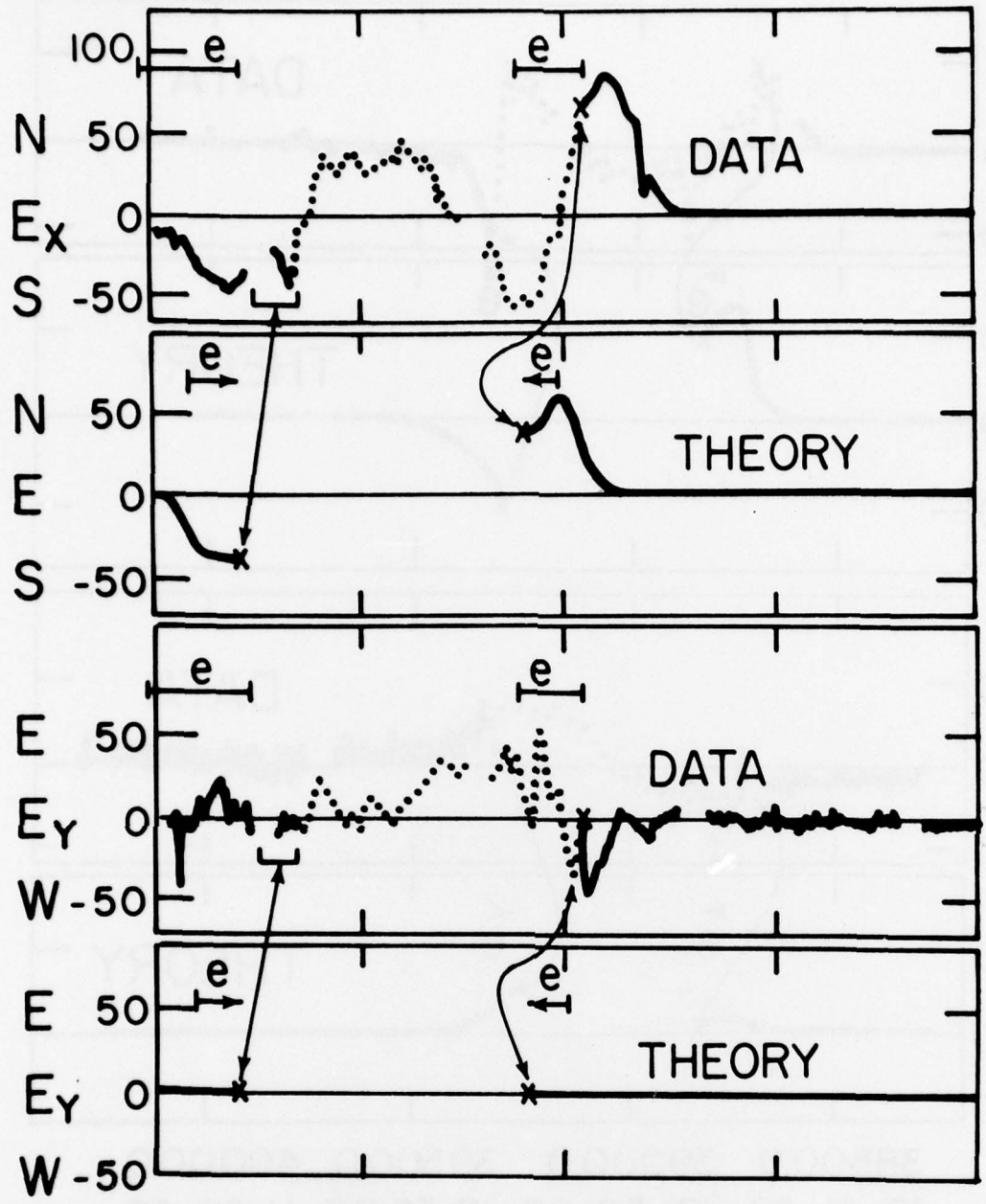

GMT	41500.0	42000.0	42500.0	43000.0	43500.0
GMT	11:31:40	11:40:00	11:48:20	11:56:40	12:05:00
ALT	995.28	1236.43	1358.18	1371.19	1249.18
MLT	6.84	3.92	19.27		
ILAT	63.07	87.28	66.68	42.23	20.03

ORBIT 4079 B SOUTH

Figure 7e

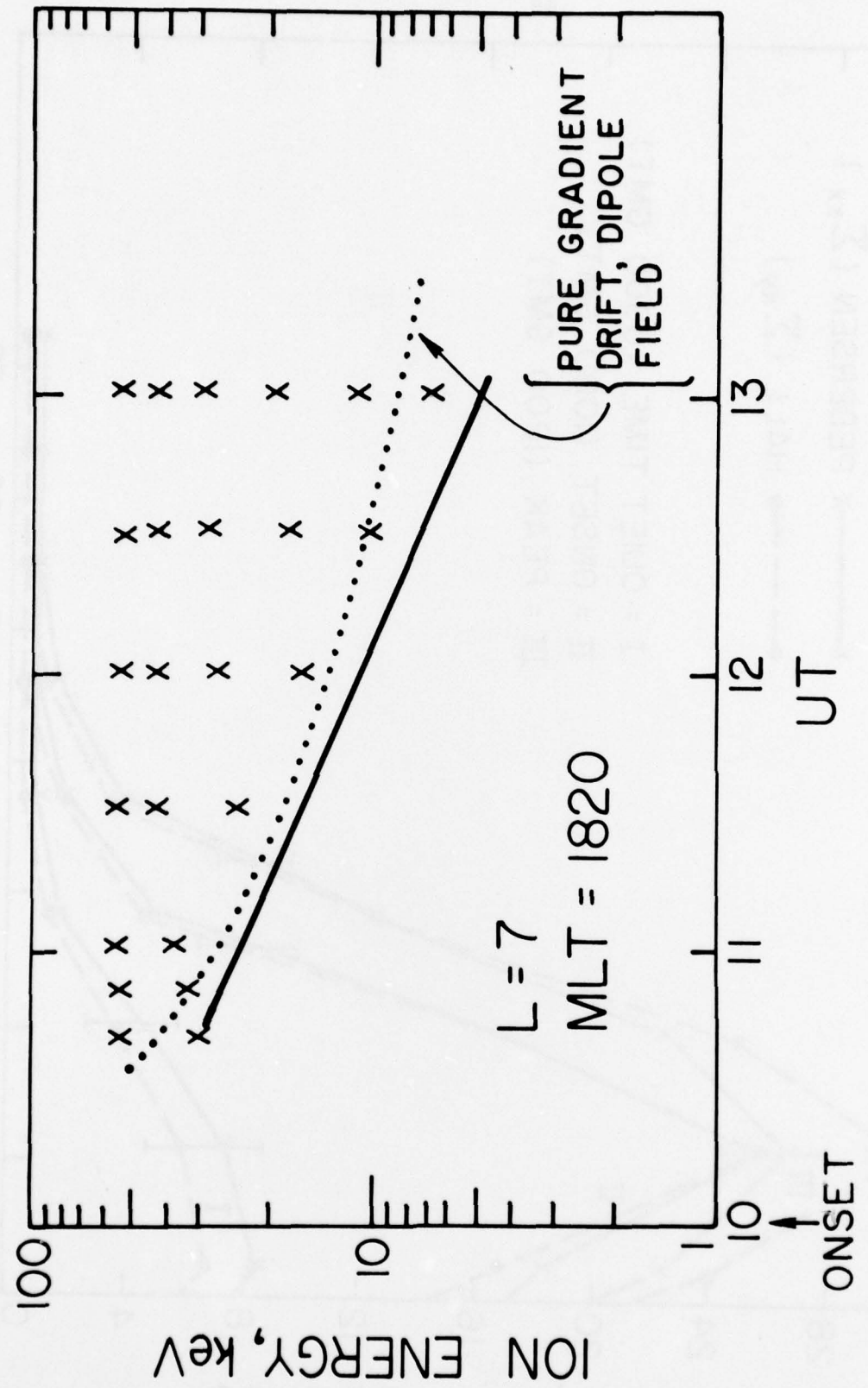
ION ENERGY, keV
100
10
1
10
11
12
13
UT
ONSET
L=7
MLT = 1820
PURE GRADIENT
DRIFT, DIPOLE
FIELD

Figure 8

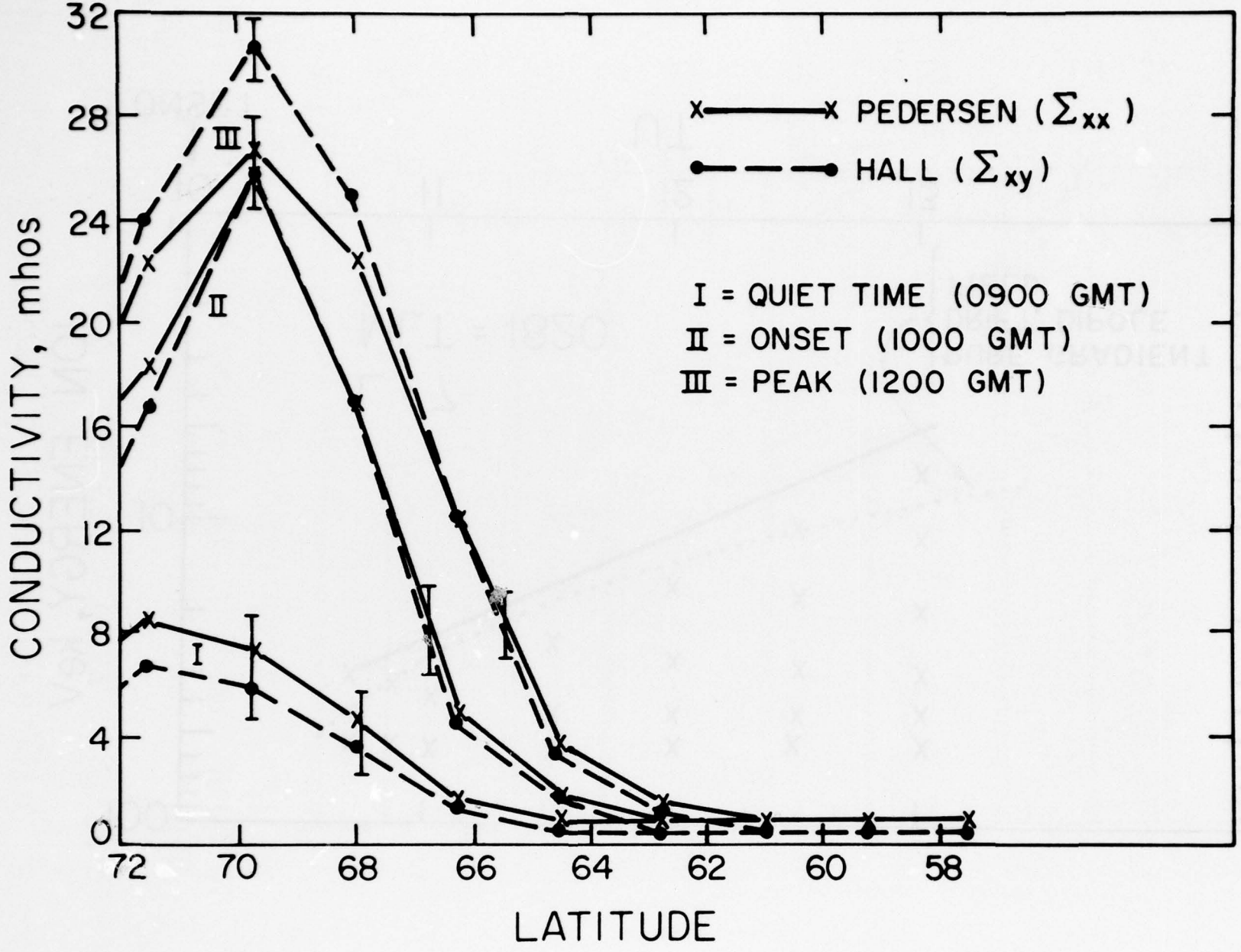
32
28
24
20
16
12
8
4
0
CONDUCTIVITY, mhos
72
70
68
66
64
62
60
58
LATITUDE
PEDERSEN (Σ_{xx})
HALL (Σ_{xy})
I = QUIET TIME (0900 GMT)
II = ONSET (1000 GMT)
III = PEAK (1200 GMT)
I
II
III

Figure 9

REFERENCES

Axford, W. I., Magnetospheric convection, Rev. Geophys., 7, 421, 1969.

Axford, W. I., and C. O. Hines, A unifying theory of high-latitude geophysical phenomena and geomagnetic storms, Can. J. Phys., 39, 1433, 1961.

Block, L. P., On the distribution of electric fields in the magnetosphere, J. Geophys. Res., 71, 855, 1966.

Chen, A. J., Penetration of low-energy protons deep into the magnetosphere, J. Geophys. Res., 75, 2458, 1970.

Cole, K. D., On solar-wind generation of polar geomagnetic disturbance, Geophys. J., 6, 103, 1961.

DeForest, S. E., and C. E. McIlwain, Plasma clouds in the magnetosphere, J. Geophys. Res., 76, 3587, 1971.

Dungey, J. W., Interplanetary magnetic field and the auroral zones, Phys. Rev. Letters, 6, 47, 1961.

Fejer, J. A., Theory of geomagnetic daily disturbance variations, J. Geophys. Res., 69, 123, 1964.

Harel, M., and R. A. Wolf, Convection, in Physics of Solar-Planetary Environments, Vol. II, ed. D. J. Williams, Amer. Geophys. Un., Washington, D.C., p. 617, 1976.

Heelis, R. A., W. B. Hanson and J. L. Burch, Ion convection velocity reversals in the dayside cleft, J. Geophys. Res., 81, 3803, 1976.

Heppner, J. P., Empirical models of high-latitude electric fields, J. Geophys. Res., 82, 1115, 1977.

Jaggi, R. K., and R. A. Wolf, Self-consistent calculation of the motion of a sheet of ions in the magnetosphere, J. Geophys. Res., 78, 2852, 1973.

Karlson, E. T., Streaming of plasma through a magnetic dipole field, Phys. Fluids, 6, 708, 1963.

Kennel, C. F., Consequences of a magnetospheric plasma, Rev. Geophys., 7, 379, 1969.

Kivelson, M. G., Magnetospheric electric fields and their variation with geomagnetic activity, Rev. Geophys. Space Phys. 14, 189, 1976.

Konradi, A., C. L. Semar, and T. A. Fritz, Substorm-injected protons and electrons and the injection boundary model, J. Geophys. Res., 80, 543, 1975.

Mal'tsev, Yu. P., The effect of ionospheric conductivity on the convection system in the magnetosphere, Geomag. Aeron., 4, 128, 1974.

McIlwain, C. E., Substorm injection boundaries, in Magnetospheric Physics, ed. B. M. McCormac, D. Reidel, Dordrecht-Holland, p. 143, 1974.

McPherron, R. L., C. T. Russell and M. P. Aubry, Satellite studies of magnetospheric substorms on August 15, 1968. 9. Phenomenological model for substorms, J. Geophys. Res., 78, 3131, 1973.

Olson, W. P., and K. A. Pfitzer, A quantitative model of the magnetospheric magnetic field, J. Geophys. Res., 79, 3739, 1974.

Rees, M. H., and R. A. Jones, Time-dependent studies of the aurora-II. spectroscopic morphology, Planet. Space Sci., 21, 1213, 1973.

Rishbeth, H. and O. K. Garriott, Introduction to Ionospheric Physics (Academic Press: New York), 1969.

Roederer, J. G., and E. W. Hones, Jr., Motion of magnetospheric particle clouds in a time-dependent electric field model, J. Geophys. Res., 79, 1432, 1974.

Rowe, J. F., and J. D. Mathews, Low-latitude nighttime E-region conductivities, J. Geophys. Res., 78, 7461, 1973.

Schield, M. A., J. W. Freeman and A. J. Dessler, A source for field-aligned currents at auroral latitudes, J. Geophys. Res., 74, 247, 1969.

Smiddy, M., M. C. Kelley, W. Burke, F. Rich, R. Sagalyn, B. Shumann, R. Hays and S. Lai, Intense poleward-directed electric fields near the ionospheric projection of the plasmapause, Geophys. Res. Lett., 4, 543, 1977.

Southwood, D. J., The role of hot plasma in magnetospheric convection, to be published in J. Geophys. Res., 1977.

Southwood, D. J., and R. A. Wolf, An assessment of the role of precipitation in magnetospheric convection, in preparation, 1977.

Spiro, R. W., R. A. Heelis, and W. B. Hanson, Ion convection and the formation of the midlatitude F-region ionospheric trough, submitted to J. Geophys. Res., 1977.

Stern, D. P., Large-scale electric fields in the earth's magnetosphere, Rev. Geophys. Space Phys., 15, 156, 1977.

Swift, D. W., Possible mechanisms for formation of the ring current belt, J. Geophys. Res., 76, 2276, 1971.

Vasyliunas, V. M., A mathematical model of plasma motions in the magnetosphere, Trans. Am. Geophys. Un., 49, 232, 1968.

Vasyliunas, V. M., Mathematical models of magnetospheric convection and its coupling to the ionosphere, in Earth's Particles and Fields in the Magnetosphere, ed. B. M. McCormac, (D. Reidel, Dordrecht-Holland), p. 60, 1970.

Vasyliunas, V. M., The interrelationship of magnetospheric processes, in Earth's Magnetospheric Processes, ed. B. M. McCormac, (D. Reidel, Dordrecht-Holland), p. 29, 1972.

Volland, H., Models of global electric fields within the magnetosphere, Ann. Geophys., 31, 154, 1975.

Winningham J. D., F. Yasuhara, S-I. Akasofu and W. J. Heikkila, The latitudinal morphology of 10-ev to 10-kev electron fluxes during magnetically quiet and disturbed times in the 2100-0300 MLT Sector, J. Geophys. Res., 3148-3171, 1975.

Wolf, R. A., Effects of ionospheric conductivity on convective flow of plasma in the magnetosphere, J. Geophys. Res., 75, 4677, 1970.

Wolf, R. A., Calculations of magnetospheric electric fields, in Magnetospheric Physics, ed. B. M. McCormac, (D. Reidel, Dordrecht-Holland), p. 167, 1974.

Wolf, R. A., Ionosphere-magnetosphere coupling, Space Sci.Rev., 17, 537, 1975.

Wolf, R. A., and R. K. Jaggi, Can the magnetospheric electric field penetrate to the low-latitude ionosphere? Comm. Astrophys. Space Phys., 5, 99, 1973.

Yasuhara, F., and S.-I. Akasofu, Field-aligned currents and ionospheric electric fields, J. Geophys. Res., 82, 1279, 1977.

SCIENTIFIC REPORTS

M. Harel and R. A. Wolf, New Model Calculations of a Typical Field Configuration for the Magnetosphere, presented at Fall 1976 AGU Meeting, San Francisco, California, December, 1976.

Abstract: First results of a new generation of computer models will be presented, covering the region $L \leq 10$. This initial run, which is intended to represent average conditions, is a preliminary to detailed simulations of specific events. A realistic potential distribution along the polar cap boundary was chosen with 50 kV cross-polar-cap potential drop. We have self-consistently computed the motion of a plasma sheet with a realistic energy spectrum. Our new work confirms the earlier result that low L-values are shielded from the convection electric field by a "shielding layer", namely, the inner edge of the plasma-sheet/ring-current region. The location and thickness of the shielding layer is computed self-consistently, an improvement over previous calculations in which the layer was assumed infinitely thin. Our ionospheric-conductivity model changes with time as the plasma sheet moves, but our magnetic-field model does not change. In this first run, neutral wind and precipitation are also neglected. Preliminary results yield potential distributions that resembe earlier models with infinitely thin shielding layer; the computed layer's thickness quickly becomes small, disregarding the highest energy components of the plasma-sheet protons.

M. Harel, R. A. Wolf and H. K. Hills, Self-consistent model calculations of magnetospheric electric fields, presented at Spring AGU meeting, Washington, D.C., May 30-June 3, 1977.

We present the latest in a continuing series of computer models of convective plasma flow in the inner magnetosphere ($L \leq 10$). The present models self-consistently include the electric-field effects of gradient-drift currents carried by

a plasma sheet with a realistic energy spectrum. Birkeland currents and horizontal ionospheric currents are included, but we neglect neutral winds and time-dependent magnetic fields, as well as loss of plasma-sheet particles by precipitation. We ran the present models for several hours magnetosphere time assuming the solar-wind-induced potential drop across the polar cap to be constant in time. The system came close to equilibrium. The inner edge of the plasma sheet came to rest at a geocentric distance of 6 - 7 R_E on the nightside, for the assumed polar cap potential drop of 50 KV. The average thickness of the shielding layer was of the order of one degree invariant latitude. The computed Birkeland currents in and out of the low-latitude part of the auroral zone have a local-time dependence and an order of magnitude that are in general agreement with TRIAD measurements. The computed strength of these currents per unit length is somewhat smaller on the nightside than on the dayside, for the conditions simulated (low magnetic activity, near equinox).

M. Harel, R. A. Wolf, and H. K. Hills, "Model calculation of magnetospheric convection including precipitation and time-dependent magnetic fields," presented at IAGA Meeting, Seattle, 22 August - 3 September, 1977.

Abstract: Results of our computer model will be presented, including, for the first time, electron precipitation and time-dependent magnetic fields. Our magnetic-field model maintains approximate pressure balance at the plasma sheet's inner edge, which moves in time. Electron precipitation is introduced in a quantitative way by assuming strong pitch-angle diffusion.

As in our earlier work, we include Birkeland currents and horizontal ionospheric currents but neglect parallel electric fields. A 50 kV cross-polar-cap potential drop is assumed as a boundary condition. We will compare these new results with previous model calculations. Relevance of the

results to the rapid-trough-flow phenomenon will also be discussed.

M. Harel, and R. A. Wolf, "Model calculation of electric fields in the magnetosphere," paper presented at IAGA Meeting, Seattle, 22 August - 3 September 1977

Abstract: For several years we have been working toward an accurate computer model of the inner magnetosphere ($L \leq 10$). We have been gradually improving our model by self-consistently adding physical features neglected in the previous generations of models. Some of these additional processes were a better conductivity model, a realistic energy spectrum for plasma-sheet particles and, most recently, electron precipitation and time dependent magnetic fields.

Starting from the equations for conservation of currents and particles in the ionosphere and the magnetosphere, and applying as a boundary condition a 50 kV potential drop across the polar cap, we have self consistently computed the motion of a plasma-sheet with multiple energies. We will present samples of recent model calculations, including some resulting from the latest version of our program, which includes time-dependent magnetic fields and electron precipitation. This will be the basis for our first effort at detailed modeling of substorm observed in the magnetosphere.

SCIENTISTS CONTRIBUTING TO THE PROJECT

M. Harel
R. A. Wolf
P. H. Reiff
H. K. Hills
A. C. Calder

VISITS TO AFGL

R. A. Wolf visited the Air Force Geophysical Laboratory 23-24 March to learn about the data being returned from satellite S3-2, to discuss possible interpretations, and to become more familiar with the technicalities of DMSP photographs.

P. H. Reiff visited the Air Force Geophysical Laboratory 11-15 July to obtain and discuss electric-field and electron flux data from satellite s3-2 and to examine the originals of certain DMSP photographs that we used for calibration purposes.

OTHER TRAVEL

R. A. Wolf attended a meeting of the SWAMP organization (Southwest Area Magnetospheric Physics) at the University of Texas at Dallas January 7, 1977, to discuss magnetospheric convection, rapid trough flows and other topics in magnetospheric physics.

H. K. Hills attended the spring AGU meeting in Washington, D.C., 30 May to 3 June 1977 to attend various sessions relevant to the contract and to discuss with R. R. Vondrak the Chatanika-radar data used in calibrating DMSP photos.

OTHER GRANTS AND CONTRACTS

The overall project of computer simulation of the inner magnetosphere during observed events is supported by several grants and contracts besides F19628-77-C-0012, specifically the following: NSF grant ATM74-21185, Air Force Contract F19628-77-C-005, and NASA grants NGR 44-006-012 and NGL 44-006-012. Different grants and contracts support different aspects of the work. Contract F19628-77-C-0012 has supported the conductivity modeling and the cold-plasma modeling. It has also supported part of the analysis of S3-2 data and part of the development of the basic program.

FISCAL INFORMATION

Of the total funds of $25,000 authorized for 12 months, approximately 100% was expended after 12 months: 100% of the work has been completed.

FINAL COST DATA

Labor Elements	Planned	Actual
Principal Investigator (R. A. Wolf)	$2178	$2433
Co-Investigator (H. K. Hills)	6416	7396
Research Associate (M. Harel)	3501	2773
Support Staff	1060	614
TOTAL LABOR	$13155	$13216
Other Expenses		
Reproduction, Telephone, Postage	$ 300	$ 256
Fringe Benefits	1449	1507
Computer	1300	1331
Travel	1125	923
Other	41	18
TOTAL OTHER EXPENSES	$ 4215	$ 4034
Overhead	$ 7630	$ 7665
GRAND TOTAL	$25000	$24915

PROPERTY AND EQUIPMENT ACQUIRED: NONE